Accurate Deterministic Projection Methods for Stiff Detonation Waves

Alina Chertock*, Shaoshuai Chu†, and Alexander Kurganov‡

Abstract

We study numerical approximations of the reactive Euler equations of gas dynamic. In addition to shock, contact and rarefaction waves, these equations admit detonation waves appearing at the interface between different fractions of the reacting species. It is well-known that in order to resolve the reaction zone numerically, one has to take both space and time stepsizes to be proportional to the reaction time, which may cause the numerical method to become very computationally expensive or even impractical when the reaction is fast. Therefore, it is necessary to develop underresolved numerical methods, which are capable of accurately predicting locations of the detonation waves without resolving their detailed structure. One can distinguish between the *stiff* and *extremely stiff* cases. While in the former case, the reaction time is very small, in the latter one, it is assumes to occur instantaneously.

In [A. Kurganov, in Hyperbolic problems: theory, numerics, applications, Springer, Berlin, 2003], we proposed a simple underresolved method—an accurate deterministic projection (ADP) method—for one-dimensional hyperbolic systems with stiff source terms including the reactive Euler equations in the extremely stiff regime. In this paper, we extend the ADP method to the (non-extremely) stiff case, to the multispecies detonation model as well as to the two-dimensional reactive Euler equations in all of the aforementioned regimes. We demonstrate the accuracy and robustness of the proposed ADP method on a number of numerical experiments.

Key words: stiff detonation waves, reactive Euler equations, splitting method, deterministic projection method, central-upwind scheme, multispecies detonation.
AMS subject classification: 76M12, 65M08, 76V05, 35L65, 35L67.

1 Introduction

We study numerical methods for hyperbolic systems of balance laws with very stiff source terms. In the two-dimensional (2-D) case, such systems read as

$$\boldsymbol{U}_t + \boldsymbol{F}(\boldsymbol{U})_x + \boldsymbol{G}(U)_y = \boldsymbol{S}(\boldsymbol{U}, \varepsilon), \tag{1.1}$$

*Department of Mathematics, North Carolina State University, Raleigh, NC 27695, USA; chertock@math.ncsu.edu

†Department of Mathematics, Southern University of Science and Technology, Shenzhen, 518055, China; 11930702@mail.sustech.edu.cn

‡Department of Mathematics, SUSTech International Center for Mathematicsi and Guangdong Provincial Key Laboratory of Computational Science and Material Design, Southern University of Science and Technology, Shenzhen, 518055, China; alexander@sustech.edu.cn

where, $\boldsymbol{U}$ is an unknown function of space variables x and y and a time variable t, $\boldsymbol{F}$ and $\boldsymbol{G}$ are given flux functions and $\boldsymbol{S}$ is a source term, which depends on the stiffness parameter $0<\varepsilon\ll 1$. In particular, we consider an inviscid, compressible, reacting flow, governed by the reactive Euler equations, which, in the single reaction case, have the following form:

$$\begin{pmatrix}\rho\\ \rho u\\ \rho v\\ E\\ \rho z\end{pmatrix}_t+\begin{pmatrix}\rho u\\ \rho u^2+p\\ \rho uv\\ u(E+p)\\ \rho uz\end{pmatrix}_x+\begin{pmatrix}\rho v\\ \rho uv\\ \rho v^2+p\\ v(E+p)\\ \rho vz\end{pmatrix}_y=\begin{pmatrix}0\\ 0\\ 0\\ 0\\ -\rho zK(\tau;\varepsilon,\tau_c)\end{pmatrix}. \tag{1.2}$$

Here, the dependent variables ρ, u, v, E and z are the density, x- and y-velocities, total energy and the fraction of unburnt gas, respectively. The system is completed through the following equation of state (EOS):

$$p=(\gamma-1)\left[E-\frac{\rho}{2}(u^2+v^2)-q_0\rho z\right], \tag{1.3}$$

where the parameters γ and q_0 represent the specific heat ratio and chemical heat release, respectively. On the right-hand side (RHS) of (1.2), $\tau:=p/\rho$ is the temperature. Finally, the reaction can be modeled by either the Arrhenius kinetic term,

$$K(\tau;\varepsilon,\tau_c)=\frac{1}{\varepsilon}e^{-\tau_c/\tau}, \tag{1.4}$$

where τ_c is the ignition temperature and ε is the reaction time, or even stiffer Heaviside kinetics term [36]:

$$K(\tau;\varepsilon,\tau_c)=\frac{1}{\varepsilon}H(\tau-\tau_c)=\begin{cases}\dfrac{1}{\varepsilon}, & \text{if } \tau\ge\tau_c,\\ 0, & \text{otherwise.}\end{cases} \tag{1.5}$$

The system (1.2), (1.3) with the kinetic term $K(\tau;\varepsilon,\tau_c)$ given by either (1.4) or (1.5) is a hyperbolic system of balance laws whose solutions contain shock, contact and rarefaction waves. In addition, in the studied stiff regimes, it also admits detonation waves appearing at the interface between the burnt and unburnt fractions of the gas. It is well-known that in order to resolve the reaction zone numerically, one has to take both spatial ($\Delta x,\Delta y$) and temporal (Δt) stepsizes to be proportional to the reaction time ε, which may cause the numerical method to become very computationally expensive or even impractical when the reaction is fast, that is, when $\Delta x/\varepsilon\gg 1$, $\Delta y/\varepsilon\gg 1$ and $\Delta t/\varepsilon\gg 1$. Therefore, it is necessary to develop underresolved numerical methods, which are capable of accurately predicting locations of the detonation waves without resolving their detailed structure. One can distinguish between the stiff and extremely stiff cases. While in the former case, the reaction time ε is very small, in the latter one, it is assumes to occur instantaneously ($\varepsilon\to 0$).

Designing an accurate underresolved numerical method for the general system (1.1) with a very small ε (or, in particular, for the reactive Euler system in either stiff or extremely stiff regime) is a rather challenging task. Since the system is stiff, it is natural that one may wish to use an operator splitting (fractional step) method; see, e.g., [28, 29]. The latter can be implemented by considering the following two subsystems:

$$\boldsymbol{U}_t+\boldsymbol{F}(\boldsymbol{U})_x+\boldsymbol{G}(\boldsymbol{U})_y=\boldsymbol{0} \tag{1.6}$$

and

$$\boldsymbol{U}_t = \boldsymbol{S}(\boldsymbol{U}, \varepsilon). \tag{1.7}$$

Then, assuming that $\boldsymbol{U}(x,t)$ is available at time t, an approximate solution at the next time level $t+\Delta t$ is given by

$$\boldsymbol{U}(x,y,t+\Delta t) = S_{\mathcal{P}}(\Delta t) S_{\mathcal{H}}(\Delta t) \boldsymbol{U}(x,y,t),$$

where $S_{\mathcal{H}}$ and $S_{\mathcal{P}}$ denote the solution operators for the subsystems (1.6) and (1.7), respectively.

The hyperbolic system of conservation laws (1.6) can be solved by any (stable and sufficiently accurate) shock-capturing method. In this paper, we use the second-order central-upwind scheme briefly described in Appendix A. Central-upwind schemes are Riemann-problem-solver-free Godunov-type schemes for general multidimensional hyperbolic systems of conservation laws. These schemes were first proposed in [25] and then further developed in [22–24, 26].

The step of solving the ODE (1.7) requires a special attention. In the extremely stiff case, the solution operator $S_{\mathcal{P}}$ reduces to the projection of the computed solution onto an equilibrium state:

$$\boldsymbol{U} \mapsto \mathcal{P}\boldsymbol{U}, \tag{1.8}$$

where $\boldsymbol{S}(\mathcal{P}\boldsymbol{U}, \varepsilon) \equiv \boldsymbol{0}$. In a less stiff case, one has to solve the ODE (1.7) with a very small, but yet finite ε. Though this solution may be very close to the projected one given by (1.8), the difference between the stiff and extremely stiff cases is sometimes significant (especially in the multispecies case considered in §4) and a sophisticated stiff ODE solver may be required.

Even though the operator splitting method is very simple, it has a major drawback: If the deterministic projection operator described in §2.1 is used in (1.8), this approach may lead to a spurious weak detonation wave that travels with a nonphysical propagation speed (the same phenomena will be observed if the ODE (1.7) is solved in the case of a very small ε disregarding of the ODE solver used). This occurs since shock-capturing methods smear discontinuities, and as soon as the nonphysical value of the temperature in this numerical layer is above the ignition temperature, a certain part of the gas may get numerically burnt prematurely. This peculiar numerical phenomenon was first observed in [10, 11], and since then it has attracted lots of attention; see, e.g., [4, 5, 7, 15, 27, 31]. In order to fix this numerical problem, the ignition temperature was artificially increased in [6], or replaced with uniformly distributed random variable; see, e.g., random projection, [1, 2], or random choice, [9], method. Numerical methods using overlapping grids and block-structured adaptive mesh refinement for high-speed reactive flow in complex geometries were proposed in [17, 18]. Other, more complicated, but rather successful approaches have been proposed in [8, 12, 16, 33, 35, 37, 38]. We refer the reader to [3, 37, 38] for the extensions of some of the aforementioned numerical methods to the case of multispecies detonation.

A simple and robust alternative to the aforementioned approaches was proposed in [20], where an accurate deterministic projection (ADP) method for one-dimensional (1-D) hyperbolic systems with extremely stiff source terms was introduced. The key idea of the ADP method for the reactive Euler equations can be described as follows. In order to avoid numerical smearing of the profile of z, we only solve the equations for the density, momentum and energy at the hydrodynamics substep $S_{\mathcal{H}}$. The values of z are then evolved in time only during the projection substep $S_{\mathcal{P}}$, at which the pressure (and hence the temperature) is computed using the EOS, at which the values of z from the previous time level are used; see the details presented in the 2-D case in §2.2.

In this paper, we generalize the ADP method developed in [20] for the 1-D reactive Euler equations in the extremely stiff regime to the 2-D case and to the following settings. First, in §3,

we consider the single reaction case in the non-extremely stiff regime with either Arrhenius (1.4) or Heaviside (1.5) kinetics terms and replace the projection operator (1.8) with the a trapezoidal-like ODE solver. We then consider in §4 the multispecies detonation, for which we either directly extend the ADP solution operator (in the extremely stiff regime; §4.1) or develop a special ADP-based ODE solver (in the non-extremely stiff regime; §4.2). These extensions are carried out in both the 1-D and 2-D cases. The developed ADP methods are tested on a number of numerical examples, presented in §2.3, 3.1 and 4.3 after each section where the corresponding version of the ADP method is presented. The obtained results clearly demonstrate the high resolution and robustness of the proposed underresolved methods in both stiff and extremely stiff regimes.

2 Deterministic Projection Method: Extremely Stiff Case

In this section, we describe two deterministic projection approaches for solving the reactive Euler equations (1.2), (1.3), (1.5) in an extremely stiff regime.

2.1 "Standard" Deterministic Projection Method

We begin with a "standard" deterministic projection approach. For simplicity, we consider a rectangular computational domain covered by a uniform spatial mesh consisting of the cells $C_{j,k}$ centered at $(x_j,y_k):=(j\Delta x,k\Delta y)$ and assume that the computed solution is realized in terms of its cell averages, $\overline{\boldsymbol{U}}^n_{j,k}=\dfrac{1}{\Delta x\Delta y}\int_{C_{j,k}}\boldsymbol{U}(x,y,t^n)\,\mathrm{d}y\,\mathrm{d}x$ and available at time level $t=t^n$. In order to evolve the solution to the next time level according to the aforementioned operator splitting approach, we first use a (stable and accurate) shock-capturing method to numerically solve the homogeneous system arising at the hydrodynamics substep (1.6):

$$\begin{pmatrix}\rho\\ \rho u\\ \rho v\\ E\\ \rho z\end{pmatrix}_t+\begin{pmatrix}\rho u\\ \rho u^2+p\\ \rho uv\\ u(E+p)\\ \rho uz\end{pmatrix}_x+\begin{pmatrix}\rho v\\ \rho uv\\ \rho v^2+p\\ v(E+p)\\ \rho vz\end{pmatrix}_y=\begin{pmatrix}0\\0\\0\\0\\0\end{pmatrix}, \tag{2.1}$$

completed through the EOS (1.3). Here, we prefer to work with finite-volume methods (in particular, with the central-upwind scheme described in Appendix A), but would like to stress that the considered computational framework is general and may be used in conjunction with one's favorite shock-capturing method. The cell averages $\overline{\rho}^{n+1}_{j,k}$, $(\overline{\rho u})^{n+1}_{j,k}$, $(\overline{\rho v})^{n+1}_{j,k}$, $\overline{E}^{n+1}_{j,k}$ and $(\overline{\rho z})^{*}_{j,k}$ at the new time level $t^{n+1}:=t^n+\Delta t$ are then used to obtain $u^{n+1}_{j,k}=(\overline{\rho u})^{n+1}_{j,k}/\overline{\rho}^{n+1}_{j,k}$, $v^{n+1}_{j,k}=(\overline{\rho v})^{n+1}_{j,k}/\overline{\rho}^{n+1}_{j,k}$,

$$p^{n+1}_{j,k}=(\gamma-1)\left[\overline{E}^{n+1}_{j,k}-\frac{\overline{\rho}^{n+1}_{j,k}}{2}\Big((u^{n+1}_{j,k})^2+(v^{n+1}_{j,k})^2\Big)-q_0(\overline{\rho z})^{*}_{j,k}\right], \tag{2.2}$$

and the corresponding temperature values,

$$\tau^{n+1}_{j,k}=\frac{p^{n+1}_{j,k}}{\overline{\rho}^{n+1}_{j,k}}. \tag{2.3}$$

Notice that for the $(\overline{\rho z})^*_{j,k}$ quantities in (2.2), the upper index is not $n+1$ yet as they are going to be changed after the projection step (1.8), at which we obtain the values of z and ρz at time level $t = t^{n+1}$:

$$z^{n+1}_{j,k} = \begin{cases} 0, & \text{if } \tau^{n+1}_{j,k} \geq \tau_c, \\ 1, & \text{if } \tau^{n+1}_{j,k} < \tau_c, \end{cases} \qquad (\overline{\rho z})^{n+1}_{j,k} = \overline{\rho}^{n+1}_{j,k} \cdot z^{n+1}_{j,k}.$$

This "standard" deterministic projection method is very simple, but as mentioned in §1 it may lead to spurious, nonphysical detonation waves traveling with artificial speeds, which makes the "standard" deterministic projection method impractical. Utilizing the ADP method presented in the next section allows one to avoid such an undesirable situation.

2.2 Accurate Deterministic Projection (ADP) Method

The main reason of the failure of the "standard" deterministic projection method is that it uses nonphysical, artificial values of $(\overline{\rho z})^*_{j,k}$ obtained after the fluid dynamics substep $S_{\mathcal{H}}$ of the operator splitting method. The simplest way to prevent this undesirable situation is not to solve the (ρz)-equation at the fluid dynamics step at all. We thus modify the deterministic projection method as follows.

Once again, we assume that cell averages of the solution at time level $t = t^n$ (including the values of the fraction of unburnt gas $z^n_{j,k} = (\overline{\rho z})^n_{j,k}/\overline{\rho}^n_{j,k}$) has been already computed. We first evolve it in time by applying a (stable and accurate) shock-capturing finite-volume method to the homogeneous system that contains only the first four equations of the system (2.1):

$$\begin{pmatrix} \rho \\ \rho u \\ \rho v \\ E \end{pmatrix}_t + \begin{pmatrix} \rho u \\ \rho u^2 + p \\ \rho uv \\ u(E+p) \end{pmatrix}_x + \begin{pmatrix} \rho v \\ \rho uv \\ \rho v^2 + p \\ v(E+p) \end{pmatrix}_y = \begin{pmatrix} 0 \\ 0 \\ 0 \\ 0 \end{pmatrix}, \tag{2.4}$$

completed through the EOS (1.3). As before, the evolved cell averages $\overline{\rho}^{n+1}_{j,k}$, $(\overline{\rho u})^{n+1}_{j,k}$, $(\overline{\rho v})^{n+1}_{j,k}$ and $\overline{E}^{n+1}_{j,k}$ (but not $(\overline{\rho z})^*_{j,k}$, which is not computed now at all) are used to obtain $u^{n+1}_{j,k}$, $v^{n+1}_{j,k}$ and

$$p^{n+1}_{j,k} = (\gamma - 1)\left[\overline{E}^{n+1}_{j,k} - \frac{\overline{\rho}^{n+1}_{j,k}}{2}\Big((u^{n+1}_{j,k})^2 + (v^{n+1}_{j,k})^2\Big) - q_0\,\overline{\rho}^{n+1}_{j,k} \cdot z^n_{j,k}\right]. \tag{2.5}$$

Notice that compared with (2.2), the pressure in (2.5) is computed using the values of z from the previous time level, which is one of the crucial points in the ADP method.

The projection step is then performed as in the case of the "standard" deterministic projection method, namely, we set

$$z^{n+1}_{j,k} = \begin{cases} 0, & \text{if } \tau^{n+1}_{j,k} \geq \tau_c, \\ 1, & \text{if } \tau^{n+1}_{j,k} < \tau_c, \end{cases} \tag{2.6}$$

where the temperature values $\tau^{n+1}_{j,k}$ are obtained by (2.3).

2.3 Numerical Examples

In this section, we demonstrate the performance of the proposed ADP method and compare it with the "standard" deterministic projection (SDP) method on four 2-D numerical examples. For the 1-D numerical examples, we refer the reader to [21].

In the first three examples, we take the CFL number 0.5 (the time step Δt is determined adaptively by using the CFL condition for the homogeneous systems (2.4) and (2.1) for the ADP and SDP methods, respectively), while in the fourth example we use a smaller CFL number 0.25 to avoid small oscillations appearing when a larger time step is used.

Example 1—Detonation Wave in a Channel

We consider the initial-boundary value problem taken from [1]. The initial data,

$$(\rho(x,y,0),u(x,y,0),v(x,y,0),p(x,y,0),z(x,y,0))=\begin{cases}(\rho_l,u_l,0,p_1,0), & \text{if } x\le\xi(y),\\ (\rho_r,u_r,0,p_r,1), & \text{if } x>\xi(y),\end{cases}$$

where

$$\xi(y)=\begin{cases}0.004, & \text{if } |y-0.0025|\ge 0.001,\\ 0.005-|y-0.0025|, & \text{if } |y-0.0025|<0.001,\end{cases}$$

are given in a 2-D channel $[0,0.025]\times[0,0.005]$ with the solid wall boundary conditions at the upper and lower boundaries and free boundary conditions on the left and on the right. We take the following parameter values: $\gamma=1.4$, $q_0=5.196\times10^9$ and $\tau_c=1.155\times10^9$, and the initial values: $\rho_l=1.945\times10^{-3}$, $p_l=6.27\times10^6$, $u_l=8.162\times10^4$, $\rho_r=1.201\times10^{-3}$, $p_r=8.321\times10^5$ and $u_r=0$, which are the same as in [1].

One important feature of this solution is that the triple points travel in the transverse direction and bounce back and forth against the upper and lower walls, forming a cellular pattern.

We compute the solutions by using both the ADP and SDP methods on a uniform spatial mesh with $\Delta x=\Delta y=5\times10^{-5}$. In Figure 2.1, we show the density computed at four different times using the ADP (top row) and SDP (bottom row) methods. The ADP results are in good agreement with the results reported in [1], while the SDP solution develops a wave traveling with a nonphysical speed. This can also be clearly seen in Figure 2.2, where we show the propagation of the interface between the burnt and unburnt fractions of the gas, computed by the two studied methods.

Example 2—Radial Detonation Wave

In the second example taken from [2], we consider the initial setting, which corresponds to a circular detonation front and consists of totally burnt gas inside a semi-circle with radius 10 and totally unburnt gas outside the semi-circle and the radially symmetric initial velocities. The radially symmetric initial data are

$$(\rho,u,v,p,z)(x,y,0)=\begin{cases}(\rho_{\rm in},u_{\rm in}(x,y),v_{\rm in}(x,y),p_{\rm in},0), & \text{if } r\le10,\\ (1,0,0,1,1), & \text{if } r>10,\end{cases}\qquad r=\sqrt{x^2+y^2},$$

where $p_{\rm in}=21.53134$, $\rho_{\rm in}=1.79463$, $u_{\rm in}(x,y)=10x/r$, and $v_{\rm in}(x,y)=10y/r$. The parameters are chosen as $\gamma=1.2$, $q_0=50$ and $\tau_c=2$.

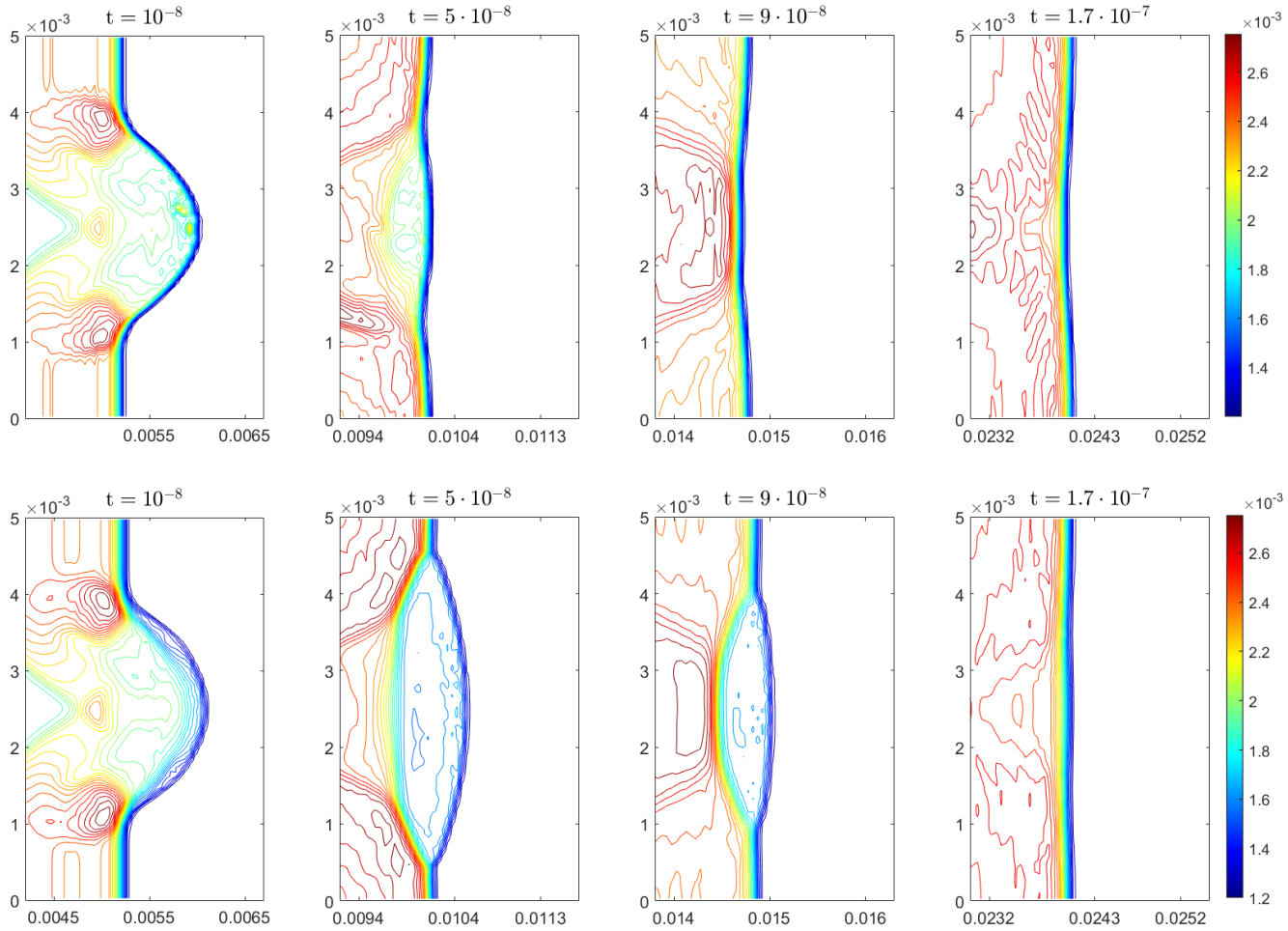

Figure 2.1: Example 1: Density ρ computed by the ADP (top row) and SDP (bottom row) methods.

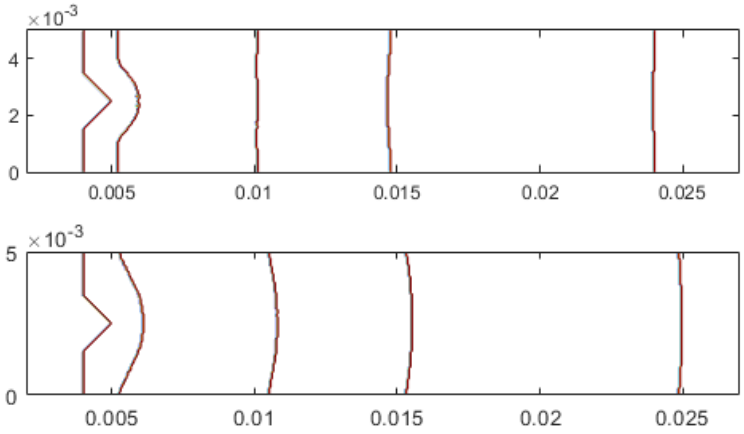

Figure 2.2: Example 1: Time evolution of the fraction of unburnt gas z computed by the ADP (top row) and SDP (bottom row) methods. In both figures, the detonation wave propagates from left to right and the interface between the burnt and unburnt fractions of the gas is shown at times $t = 0$, 10^{-8}, $5 \cdot 10^{-8}$, $9 \cdot 10^{-8}$ and $1.7 \cdot 10^{-7}$.

We take the computational domain $[-50,50]\times[0,50]$ and use a uniform spatial mesh with $\Delta x=\Delta y=1$. The solid wall boundary conditions are used along the bottom part of the domain, while the free boundary conditions are implemented at the other parts of the boundary. We have solved the problem numerically by both the ADP and SDP methods and the obtained results are reported in Figures 2.3 and 2.4.

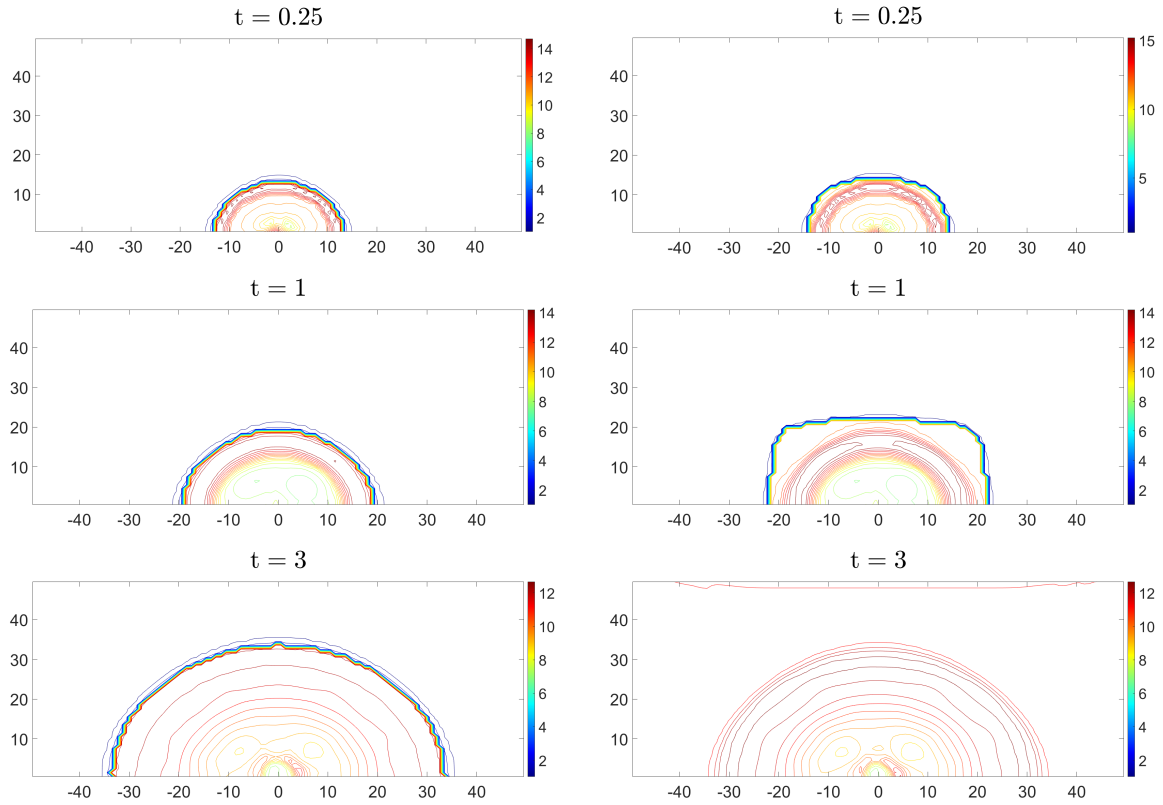

Figure 2.3: Example 2: Temperature τ computed by the ADP (left column) and SDP (right column) methods.

In Figure 2.3, we show the temperature component of the computed solution at times $t=0.25$, 1 and 3. As one can see, the ADP and SDP temperatures are totally different even at a smaller time $t=0.25$. The source of this difference can be understood by looking at the propagation of the interface between the burnt and unburnt fractions of the gas shown in Figure 2.4. As the ADP solution is in a good agreement with the solution reported in [2], we conclude that the fast wave developed by the SDP solution is a numerical artifact that can be prevented by using the proposed ADP.

Example 3—Interaction of Gas Dynamics and Detonation Waves

In the third example, we study the collision of a radially symmetric stiff detonation wave with a shock, contact discontinuity and rarefaction wave. This problem is an extension of the 1-D

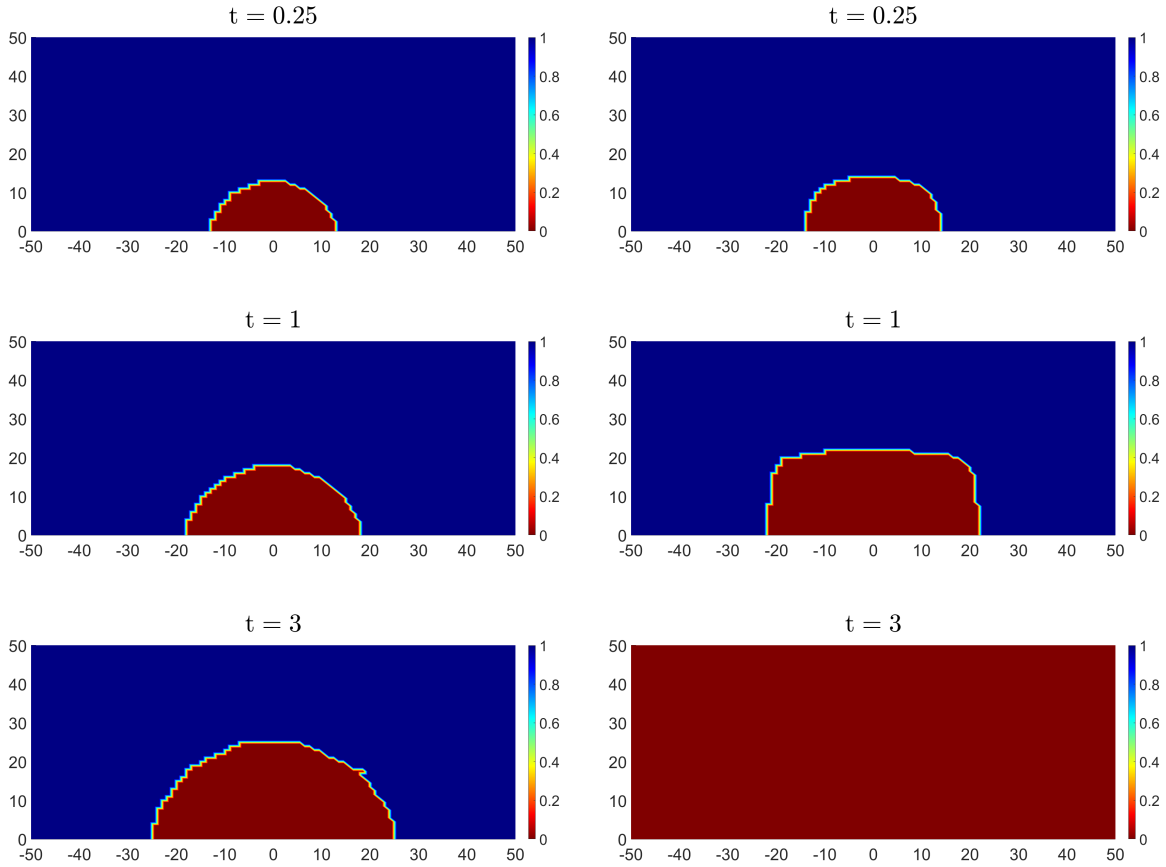

Figure 2.4: Example 2: Fraction of unburned gas z (shaded in red) computed by the ADP (left column) and SDP (right column) methods.

experiment conducted in [2, 19, 20]. We consider the following initial data:

$$(\rho, u, v, p, z)(x, y, 0) = \begin{cases} (4, 0, 0, 10, 0), & \text{if } \ x > 40, \\ (3.64282, 10\cos\theta, 10\sin\theta, 54.8244, 0), & \text{if } \ \sqrt{x^2+y^2} < 10, \\ (1, 0, 0, 1, 1), & \text{otherwise,} \end{cases}$$

where $\tan\theta = y/x$ and use the following parameters: $\gamma = 1.2$, $q_0 = 50$ and $\tau_c = 3$. We take the computational domain $[-30, 100] \times [-30, 30]$, on which we implement free boundary conditions, and use a uniform spatial mesh with $\Delta x = \Delta y = 0.5$.

The results (temperature and fraction of unburnt gas) obtained by the ADP and SDP methods at times $t = 0.25$, 1, 3, 4 and 5 are reported in Figures 2.5 and 2.6. As one can observe, both methods provide similar approximations at small times $t = 0.25$ and 1 (before the collision). At a later time $t = 3$ (after the collision with the shock, but before the collision with the rarefaction wave), the solutions start exhibiting a different behavior due to the fact that the detonation wave produced by the SDP method starts moving with an nonphysical speed; this is similar to the 1-D case studied in [20]. Finally, at times $t = 4$ and 5 (after all the collisions), the detonation wave front computed by the SDP method keeps moving to the right with the increasing nonphysical speed. At the same time, the ADP method seems to produce accurate results.

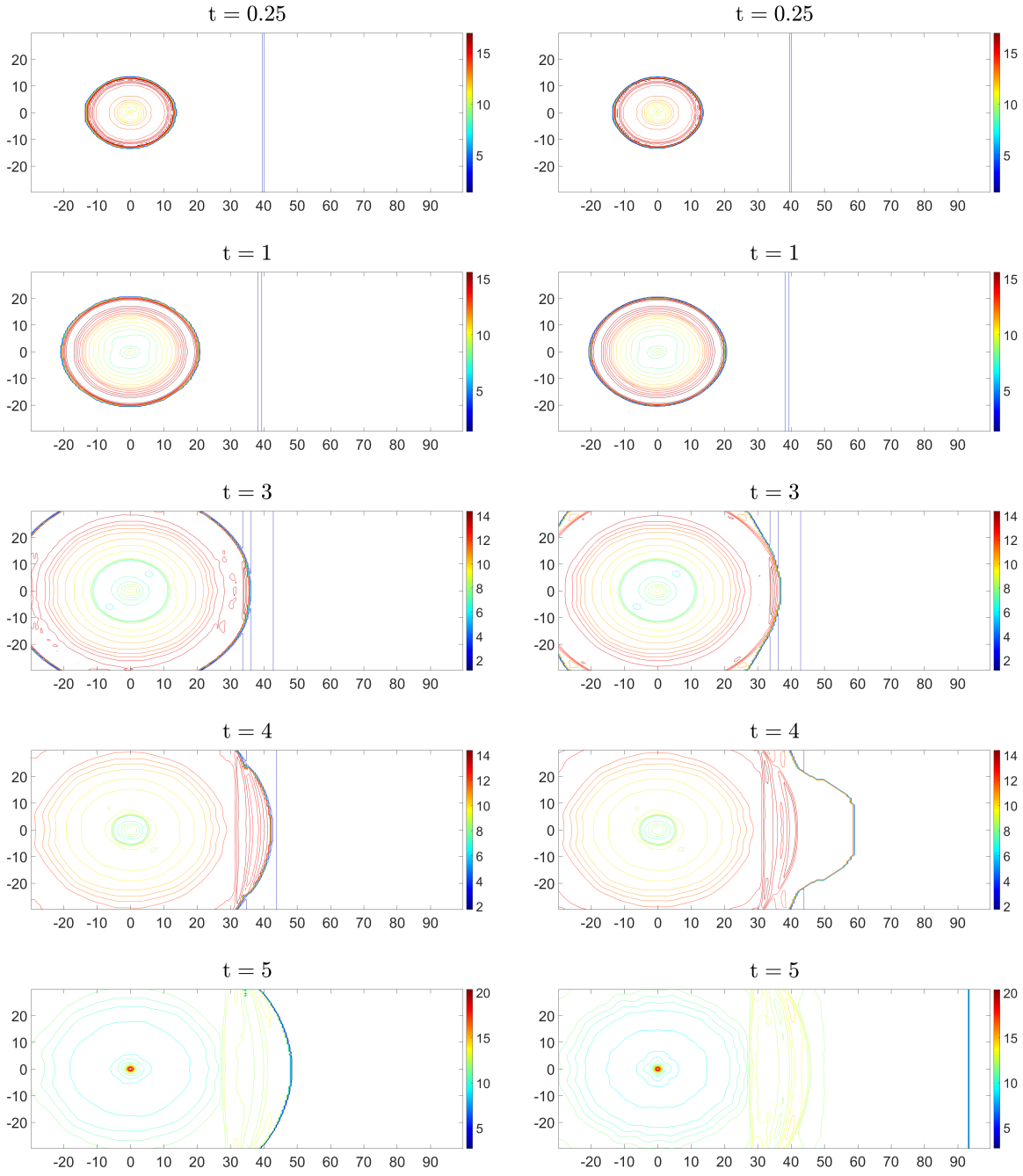

Figure 2.5: Example 3: Temperature τ computed by the ADP (left column) and SDP (right column) methods.

Example 4—Diffraction of a Detonation Wave

In the last example of this section, we consider a detonation wave in the domain $[-1,0]\times[0,1]\cup[0,3]\times[-1,1]$ with the solid walls along the top part of the boundary and along the following line segments: $\{-1\le x\le 0,\ y=0\}$, $\{x=0,\ -1\le y\le 0\}$ and $\{0\le x\le 3,\ y=-1\}$, and the open

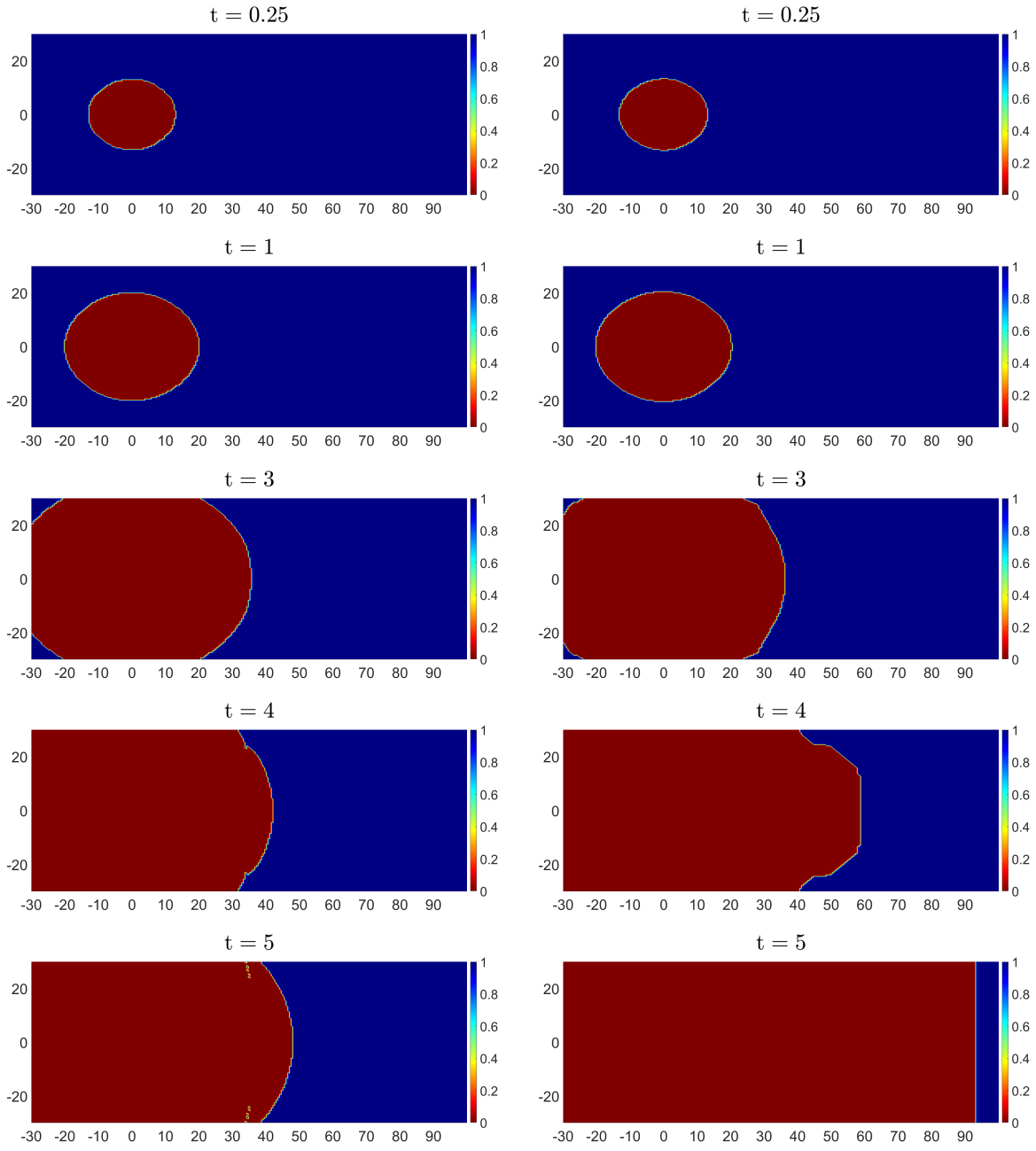

Figure 2.6: Example 3: Fraction of unburned gas z (shaded in red) computed by the ADP (left column) and SDP (right column) methods.

boundaries on the left and on the right. The initial data are

$$(\rho, u, v, p, z)(x, y, 0) = \begin{cases} (3.64282,\ 6.2489,\ 0,\ 54.8244,\ 0), & \text{if } \ x \le -0.5, \\ (1, 0, 0, 1, 1), & \text{if } \ x > -0.5, \end{cases}$$

and the parameters are the same as in Example 2: $\gamma = 1.2$, $q_0 = 50$ and $\tau_c = 2$. The initial setting is outlined in Figure 2.7.

In this example, the detonation wave initially positioned vertically at $x = -0.5$, first propagates

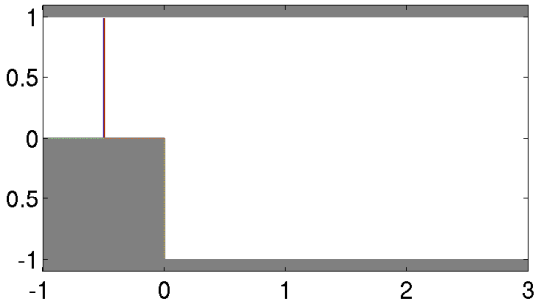

Figure 2.7: Example 4: Domain and the initial wave location.

to the right and then diffracts around a solid corner. We compute the solution at times $t = 0.2$ and 0.4 on a uniform spatial grid with $\Delta x = \Delta y = 1/100$ using both the ADP and SDP methods. The results are shown in Figures 2.8 and 2.9, where we plot the temperature and the fraction of unburnt gas fields. As one can clearly see, an artificially fast wave generated by the SDP method after the diffraction, is prevented by the use of the proposed ADP procedure.

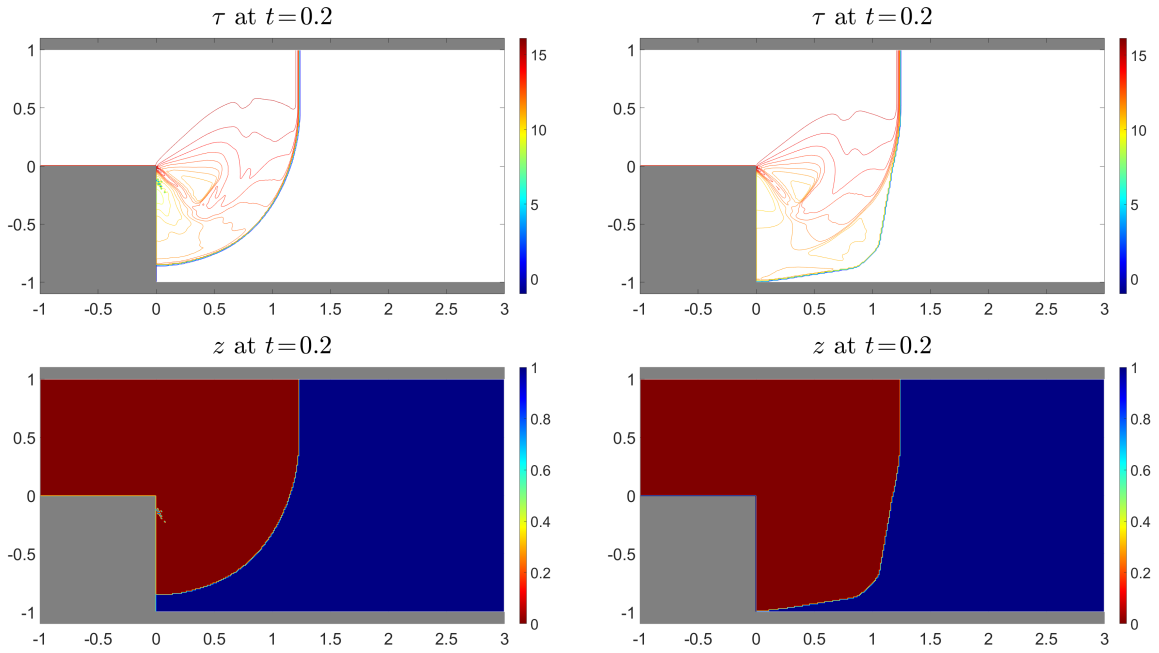

Figure 2.8: Example 4: Temperature τ (top row) and fraction of unburnt gas z (bottom row) at time $t = 0.2$ computed by the ADP (left column) and SDP (right column) methods.

3 Accurate Deterministic Projection Method: Stiff Case

We now consider a stiff, but not extremely stiff regime. In this case, instead of performing a direct projection (1.8) one has to numerically solve the stiff ODE (1.7) at the projection substep $S_{\mathcal{P}}$.

To this end, we first note that the last equation of the system (1.2) can be combined with the

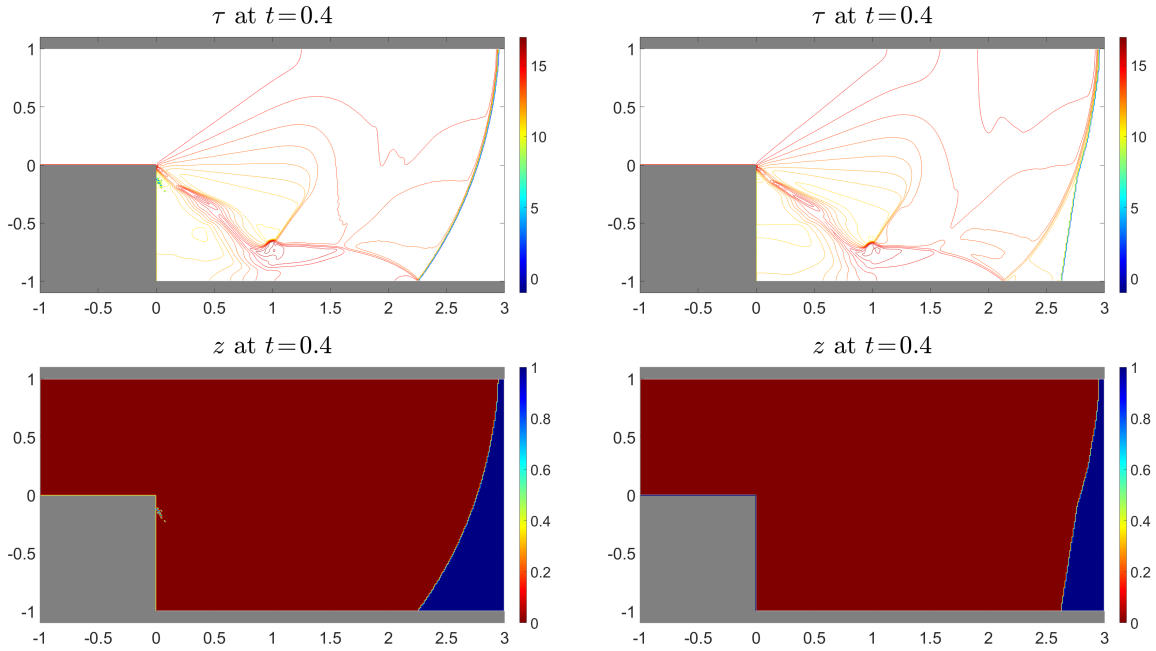

Figure 2.9: Example 4: Same as in Figure 2.8, but at time $t = 0.4$.

density equation and then recast in the nonconservative form as

$$z_t + uz_x + vz_y = -zK(\tau;\varepsilon,\tau_c).$$

Therefore, at the projection substep $S_{\mathcal{P}}$, we will have to solve the following stiff ODE:

$$z_t = -zK(\tau;\varepsilon,\tau_c), \tag{3.1}$$

where $K(\tau;\varepsilon,\tau_c)$ is given by either (1.4) or (1.5).

In order to develop a proper ODE solver for (3.1), we first rewrite it in terms of an auxiliary variable $w := \ln z$,

$$w_t = -K(\tau;\varepsilon,\tau_c), \tag{3.2}$$

and then apply the trapezoidal method to the rewritten equation (3.2). This results in

$$w^{n+1}_{j,k} = w^n_{j,k} - \frac{\Delta t}{2}\Big[K(\tau^n_{j,k};\varepsilon,\tau_c) + K(\tau^{n+1}_{j,k};\varepsilon,\tau_c)\Big],$$

which, after the backward substitution $z = e^w$, gives the following trapezoidal-like ODE method for z:

$$z^{n+1}_{j,k} = z^n_{j,k}\exp\left\{-\frac{\Delta t}{2}\Big[K(\tau^n_{j,k};\varepsilon,\tau_c) + K(\tau^{n+1}_{j,k};\varepsilon,\tau_c)\Big]\right\}, \tag{3.3}$$

where the corresponding pressure $p^{n+1}_{j,k}$ and temperature $\tau^{n+1}_{j,k}$ values are calculated using the ADP approach, namely, using (2.5) and (2.3). Notice that this ADP-like implementation of the ODE solver (3.3) is, in fact, an explicit realization of the implicit method.

3.1 Numerical Examples

In this section, we present two numerical experiments, in which we consider stiff, but not extremely stiff, 1-D and 2-D problems with the Arrhenius kinetic term. Notice that the 2-D ADP method proposed in §3 can be reduced to the 1-D case in a straightforward way. In both examples, the CFL number is chosen as 0.3.

Example 5—1-D Stiff Detonation Waves

We first consider the 1-D example taken from [33,35,38]. The initial conditions, which correspond to a burned gas on the left and unburned gas on the right, are given by

$$(\rho,u,p,z)(x,0)=\begin{cases}(1.6812,\ 2.8867,\ 21.5672,\ 0), & \text{if } x\le 10,\\ (1,0,1,1), & \text{if } x>10,\end{cases}$$

and the parameters are chosen as $\gamma=1.4$, $q_0=25$, $1/\varepsilon=16418$ and $\tau_c=15$. We take the computational domain $[0,30]$ and use a uniform spatial mesh with $\Delta x=0.1$. The density, pressure, temperature and fraction of unburnt gas, computed by both the ADP and SDP methods at $t=1.5$, are presented in Figure 3.1 together with the reference solution obtained using the ADP method on a uniform spatial mesh with $\Delta x=0.01$. As one can see, the proposed ADP method captures the detonation wave propagating with the correct speed, while the detonation wave computed by the SDP method moves faster. Also note that our results are in good agreement with those reported in [38, Example 4.1].

Example 6—2-D Stiff Detonation Waves

We now consider the 2-D example taken from [38], and take the initial conditions similar to those in Example 2, but put into the radially symmetric setting:

$$(\rho,u,v,p,z)(x,y,0)=\begin{cases}(\rho_{\rm in},u_{\rm in}(x,y),v_{\rm in}(x,y),p_{\rm in},0), & \text{if } r\le 2,\\ (1,0,0,1,1), & \text{if } r>2,\end{cases}$$

where $r=\sqrt{x^2+y^2}$, $p_{\rm in}=21.53134$, $\rho_{\rm in}=1.79463$, $u_{\rm in}(x,y)=10x/r$ and $v_{\rm in}(x,y)=10y/r$. The parameters are $\gamma=1.4$, $q_0=30$, $1/\varepsilon=20000$ and $\tau_c=15$. The computational domain is $[-10,10]\times[0,10]$ and we use a uniform mesh with $\Delta x=\Delta y=0.1$. We compute the solution using both the ADP and SDP methods until the final time $t=1$ and present the obtained density, pressure, temperature and fraction of unburnt gas along the $y=x$ 1-D cross-section in Figure 3.2. The results are plotted along with the reference solution computed by the ADP method on a uniform spatial mesh with $\Delta x=\Delta y=0.025$. As in the previous example, only the ADP method captures the detonation wave propagating with the correct speed. We would also like to point out that our results are similar to those reported in [38, Example 4.4].

4 ADP Methods for Multispecies Detonation

In this section, we extend the ADP methods described in §2.2 and §3 to the multispecies detonation; see, e.g., [3,37,38].

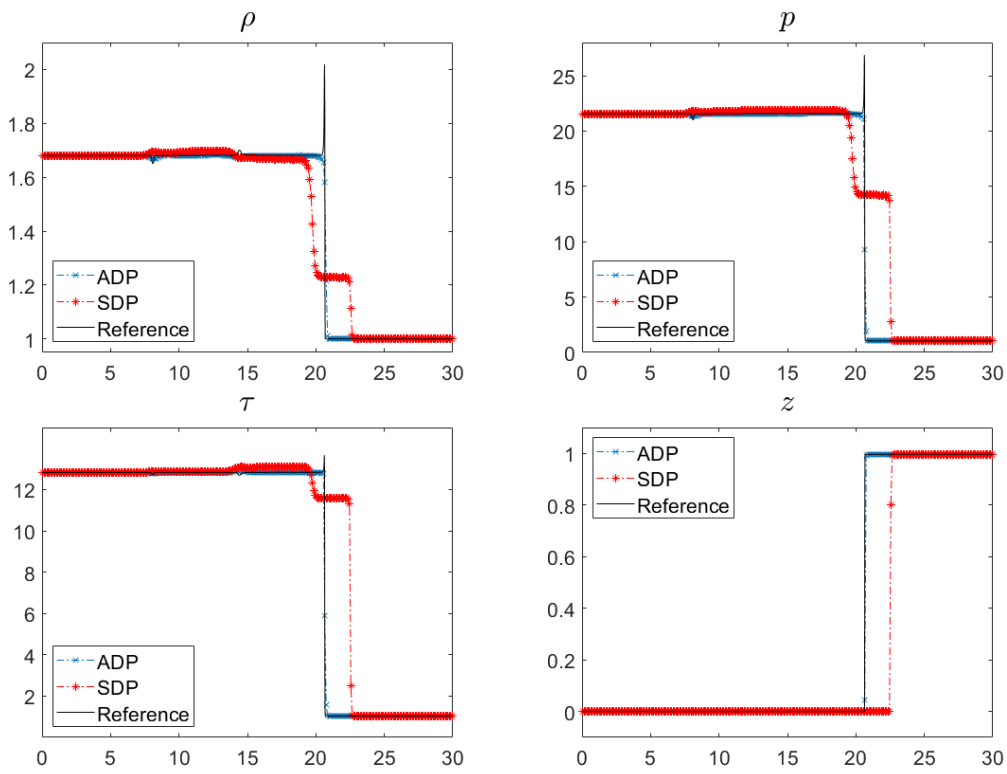

Figure 3.1: Example 5: Density (ρ), pressure (p), temperature (τ) and mass fraction (z) computed by the ADP and SDP methods.

The governing equations now read as (1.1) with

$$\boldsymbol{U} = \begin{pmatrix} \rho \\ \rho u \\ \rho v \\ E \\ \rho z_1 \\ \vdots \\ \rho z_N \end{pmatrix}, \quad \boldsymbol{F}(\boldsymbol{U}) = \begin{pmatrix} \rho u \\ \rho u^2 + p \\ \rho uv \\ u(E+p) \\ \rho u z_1 \\ \vdots \\ \rho u z_N \end{pmatrix}, \quad \boldsymbol{G}(\boldsymbol{U}) = \begin{pmatrix} \rho v \\ \rho uv \\ \rho v^2 + p \\ v(E+p) \\ \rho v z_1 \\ \vdots \\ \rho v z_N \end{pmatrix}, \quad \boldsymbol{S}(\boldsymbol{U}, \boldsymbol{\varepsilon}) = \begin{pmatrix} 0 \\ 0 \\ 0 \\ 0 \\ S_1(\boldsymbol{U}, \boldsymbol{\varepsilon}) \\ \vdots \\ S_N(\boldsymbol{U}, \boldsymbol{\varepsilon}) \end{pmatrix}, \tag{4.1}$$

where $\boldsymbol{\varepsilon} := (\varepsilon_1, \ldots, \varepsilon_N)^\top$ and

$$S_i(\boldsymbol{U}, \boldsymbol{\varepsilon}) = W_i \sum_{\ell=1}^{M} (v''_{i\ell} - v'_{i\ell}) K(\tau; \varepsilon_\ell, \tau_\ell) \prod_{j=1}^{N} \left(\frac{\rho z_j}{W_j} \right)^{v'_{j\ell}}, \quad i = 1, \ldots, N. \tag{4.2}$$

Here, M and N are the numbers of reactions and chemical species, W_i and z_i are the molecular weight and the mass fraction of the i-th chemical species, $v''_{i\ell}$ and $v'_{i\ell}$ are the stoichiometric coefficients for the i-th species appearing as a product and a reactant in the ℓ-th reaction, ε_ℓ and τ_ℓ represent the reaction time and the ignition temperature for the ℓ-th reaction, and $K(\tau; \varepsilon_\ell, \tau_\ell)$ is the kinetic term given by either (1.4) or (1.5). Finally, the mass fractions satisfy the algebraic

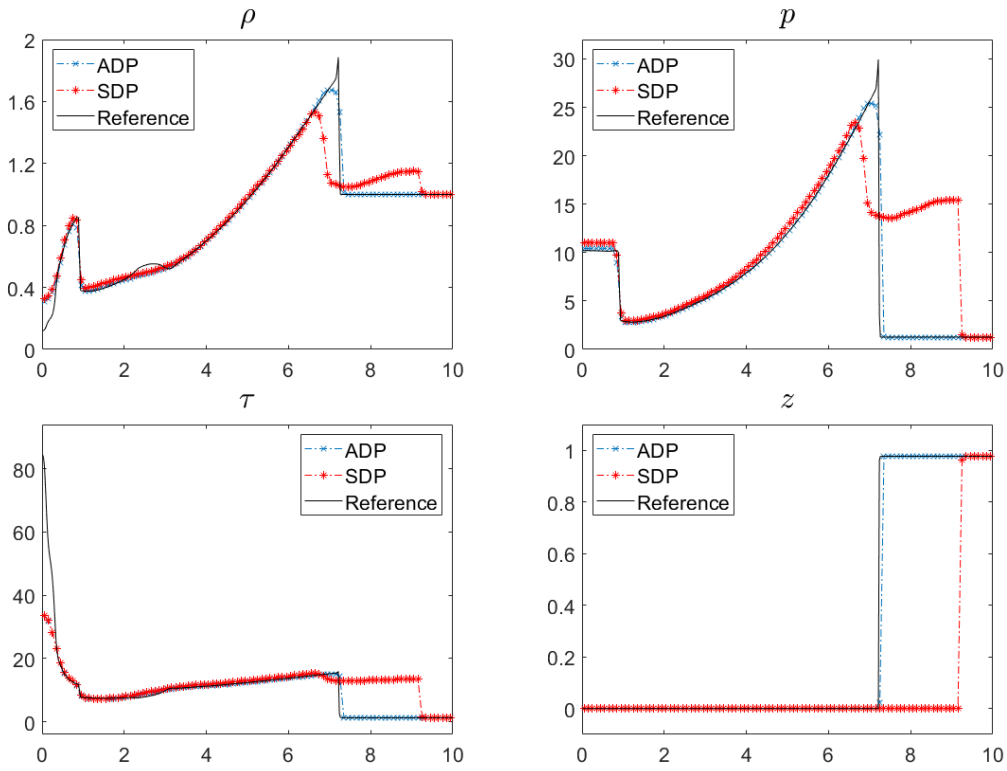

Figure 3.2: Example 6: 1-D cross-sections along the $y = x$ of the density (ρ), pressure (p), temperature (τ) and mass fraction (z) computed by the ADP and SDP methods.

relation

$$\sum_{i=1}^{N} z_i = 1, \tag{4.3}$$

and the system (1.1), (4.1)–(4.3) is completed through the following EOS:

$$p = (\gamma - 1)\Big[E - \frac{\rho}{2}(u^2 + v^2) - \sum_{i=1}^{N} q_i \rho z_i\Big]. \tag{4.4}$$

Example. To cite an example, we consider a reacting model consisting of five species and two reactions. Prototype reactions for such model are

$$\mathrm{H_2} + \mathrm{O_2} \to 2\mathrm{OH}, \qquad 2\mathrm{OH} + \mathrm{H_2} \to 2\mathrm{H_2O}, \tag{4.5}$$

with $\tau_1 \le \tau_2$ and $\mathrm{N_2}$ being a catalyst. In this case, $M = 2$, $N = 5$, $v'_{1,1} = 1$, $v'_{2,1} = 1$, $v'_{3,1} = 0$, $v'_{4,1} = 0$, $v'_{5,1} = 0$, $v'_{1,2} = 1$, $v'_{2,2} = 0$, $v'_{3,2} = 2$, $v'_{4,2} = 0$, $v'_{5,2} = 0$, $v''_{1,1} = 0$, $v''_{2,1} = 0$, $v''_{3,1} = 2$, $v''_{4,1} = 0$, $v''_{5,1} = 0$, $v''_{1,2} = 0$, $v''_{2,2} = 0$, $v''_{3,2} = 0$, $v''_{4,2} = 2$ and $v''_{5,2} = 0$. Therefore, formula (4.2) reads as

$$\begin{aligned}
S_1 &= W_1\Big[- K(\tau;\varepsilon_1,\tau_1)\Big(\frac{\rho z_1}{W_1}\Big)\Big(\frac{\rho z_2}{W_2}\Big) - K(\tau;\varepsilon_2,\tau_2)\Big(\frac{\rho z_1}{W_1}\Big)\Big(\frac{\rho z_3}{W_3}\Big)^2\Big],\\
S_2 &= W_2\Big[- K(\tau;\varepsilon_1,\tau_1)\Big(\frac{\rho z_1}{W_1}\Big)\Big(\frac{\rho z_2}{W_2}\Big)\Big],\\
S_3 &= W_3\Big[2K(\tau;\varepsilon_1,\tau_1)\Big(\frac{\rho z_1}{W_1}\Big)\Big(\frac{\rho z_2}{W_2}\Big) - 2K(\tau;\varepsilon_2,\tau_2)\Big(\frac{\rho z_1}{W_1}\Big)\Big(\frac{\rho z_3}{W_3}\Big)^2\Big].
\end{aligned} \tag{4.6}$$

The corresponding molecular weights are $W_1 = 2$, $W_2 = 32$ and $W_3 = 17$, but we will not substitute them in (4.6) until we conduct the numerical experiments reported in Example 8 below.

Note that it is unnecessary to compute the source term S_5, since N_2 is the catalyst whose mass fraction z_5 will not change during the chemical reaction. It is also unnecessary to compute the source term S_4, since z_4 can be obtained directly from (4.3) and it is equal to

$$z_4 = 1 - z_1 - z_2 - z_3 - z_5. \tag{4.7}$$

In the remaining part of §4, we will present an extension of the ADP methods to the multispecies detonation. For the simplicity of presentation, we restrict our consideration to the reactions presented in the above example.

4.1 Extremely Stiff Case

We begin with the extremely stiff case, in which the multispecies extension of the ADP method is quite straightforward. As before, the time evolution of the computed solution from time $t = t^n$ to $t = t^{n+1}$ consists of two splitting substeps. We first solve the system (2.4) to obtain the cell averages $\overline{\rho}_{j,k}^{n+1}$, $(\overline{\rho u})_{j,k}^{n+1}$, $(\overline{\rho v})_{j,k}^{n+1}$ and $\overline{E}_{j,k}^{n+1}$ and use them and the EOS (4.4) to obtain $u_{j,k}^{n+1}$, $v_{j,k}^{n+1}$ and

$$p_{j,k}^{n+1} = (\gamma - 1)\left[\overline{E}_{j,k}^{n+1} - \frac{\overline{\rho}_{j,k}^{n+1}}{2}\Big((u_{j,k}^{n+1})^2 + (v_{j,k}^{n+1})^2\Big) - \sum_{i=1}^{5} q_i\,\overline{\rho}_{j,k}^{n+1}\cdot(z_i)_{j,k}^{n}\right]. \tag{4.8}$$

We then compute the corresponding temperature values $\tau_{j,k}^{n+1}$ using (4.8) and (2.3), and generalize the ADP operator (2.6) to the multispecies case as follows:

$$(z_i)_{j,k}^{n+1} = \begin{cases} z_i^{HT}, & \text{if } \ \tau_{j,k}^{n+1} \ge \tau_2, \\ z_i^{IT}, & \text{if } \ \tau_2 > \tau_{j,k}^{n+1} \ge \tau_1, \\ z_i^{LT}, & \text{if } \ \tau_{j,k}^{n+1} < \tau_1, \end{cases} \qquad i = 1, 2, 3. \tag{4.9}$$

Here, z_i^{LT}, z_i^{IT} and z_i^{HT} are the mass fractions of the i-th chemical species in the low, intermediate and high temperature regimes, respectively. We note that when the temperature is lower than τ_1, no reactions occur, while when the temperature is higher than τ_2, then both reactions have been completed. The value of z_i^{IT} depends on the quantities of the reactants in the mixture. For the sake of brevity, we will only consider the case in which there is more hydrogen than oxygen, that is, $z_1^{LT} \ge \frac{W_1}{W_2}\, z_2^{LT}$. The values of the mass fractions z_i^{IT} are then given by

$$z_1^{IT} = z_1^{LT} - \frac{W_1}{W_2}\, z_2^{LT}, \quad z_2^{IT} = 0, \quad z_3^{IT} = \frac{2W_3}{W_2}\, z_2^{LT}.$$

Finally, we note that $(z_5)_{j,k}^{n+1} = (z_5)_{j,k}^{0}$ as the mass fraction of a catalyst remains constant during the entire reaction process, and $(z_4)_{j,k}^{n+1} = 1 - (z_1)_{j,k}^{n+1} - (z_2)_{j,k}^{n+1} - (z_3)_{j,k}^{n+1} - (z_5)_{j,k}^{n+1}$ from (4.3).

4.2 Stiff Case

In order to complete the derivation of the APD method in the stiff case, we need to develop an ODE solver for the system of ODEs with the RHS given by (4.6) (or (4.2) in the general case):

$$(z_1)_t = W_1\Big[-K(\tau;\varepsilon_1,\tau_1)\Big(\frac{z_1}{W_1}\Big)\Big(\frac{\rho z_2}{W_2}\Big) - K(\tau;\varepsilon_2,\tau_2)\Big(\frac{z_1}{W_1}\Big)\Big(\frac{\rho z_3}{W_3}\Big)^2\Big], \tag{4.10}$$

$$(z_2)_t = W_2\Big[-K(\tau;\varepsilon_1,\tau_1)\Big(\frac{z_1}{W_1}\Big)\Big(\frac{\rho z_2}{W_2}\Big)\Big], \tag{4.11}$$

$$(z_3)_t = W_3\Big[2K(\tau;\varepsilon_1,\tau_1)\Big(\frac{z_1}{W_1}\Big)\Big(\frac{\rho z_2}{W_2}\Big) - 2K(\tau;\varepsilon_2,\tau_2)\Big(\frac{z_1}{W_1}\Big)\Big(\frac{\rho z_3}{W_3}\Big)^2\Big]. \tag{4.12}$$

Equations (4.10)–(4.12) can be simplified as follows. First, it can be easily verified that

$$\Big(z_3 + \frac{2W_3}{W_1}z_1 - \frac{4W_3}{W_2}z_2\Big)_t = 0,$$

which implies that the quantity

$$c := z_3 + \frac{2W_3}{W_1}z_1 - \frac{4W_3}{W_2}z_2 \tag{4.13}$$

is independent of time. Therefore, z_3 can be expressed from (4.13) and substituted into (4.10) so that we will only need to solve a 2×2 system of ODEs consisting of (4.10) and (4.11). We then divide (4.10) and (4.11) by z_1 and z_2, respectively, introduce $w_1 := \ln z_1$ and $w_2 := \ln z_2$, and obtain the system

$$(w_1)_t = R_1, \quad (w_2)_t = R_2, \tag{4.14}$$

where

$$\begin{aligned} R_1 &= \Big[-K(\tau;\varepsilon_1,\tau_1)\Big(\frac{\rho z_2}{W_2}\Big) - K(\tau;\varepsilon_2,\tau_2)\Big(\frac{\rho z_3}{W_3}\Big)^2\Big], \quad z_3 = c - \frac{2W_3}{W_1}z_1 + \frac{4W_3}{W_2}z_2,\\ R_2 &= \Big[-K(\tau;\varepsilon_1,\tau_1)\Big(\frac{\rho z_1}{W_1}\Big)\Big]. \end{aligned} \tag{4.15}$$

We solve the ODE system (4.14), (4.15) in a predictor-corrector manner. First, we predict the solution at time $t = t^{n+1}$ using the forward Euler method, which in terms of $z_1 = e^{w_1}$ and $z_2 = e^{w_2}$ reads as

$$(z_1)^*_{j,k} = (z_1)^n_{j,k}\exp\left(\Delta t(R_1)^n_{j,k}\right), \quad (z_2)^*_{j,k} = (z_2)^n_{j,k}\exp\left(\Delta t(R_2)^n_{j,k}\right),$$

where the terms $(R_1)^n_{j,k}$ and $(R_2)^n_{j,k}$ are computed by (4.15) with $\tau^n_{j,k}$ obtained using (4.4):

$$\tau^n_{j,k} = (\gamma-1)\Big[\frac{\overline{E}^n_{j,k}}{\overline{\rho}^n_{j,k}} - \frac{1}{2}\Big((u^n_{j,k})^2 + (v^n_{j,k})^2\Big) - \sum_{i=1}^N q_i(z_i)^n_{j,k}\Big]. \tag{4.16}$$

The computed values $(z_1)^*_{j,k}$ and $(z_2)^*_{j,k}$ are then updated with the help of a special trapezoidal-like corrector, once again applied to the ODEs (4.14) and then written in terms of $z_1 = e^{w_1}$ and $z_2 = e^{w_2}$ as

$$\begin{aligned} (z_1)^{n+1}_{j,k} &= (z_1)^*_{j,k}\exp\left\{\frac{\Delta t}{2}\Big[(R_1)^n_{j,k} + (R_1)^*_{j,k}\Big]\right\},\\ (z_2)^{n+1}_{j,k} &= (z_2)^*_{j,k}\exp\left\{\frac{\Delta t}{2}\Big[(R_2)^n_{j,k} + (R_2)^*_{j,k}\Big]\right\}. \end{aligned} \tag{4.17}$$

where the terms $(R_1)^*_{j,k}$ and $(R_2)^*_{j,k}$ are computed by (4.15) with $\tau^n_{j,k}$ obtained using (4.4):

$$\tau^*_{j,k} = (\gamma - 1)\left[\frac{\overline{E}^{n+1}_{j,k}}{\overline{\rho}^{n+1}_{j,k}} - \frac{1}{2}\Big((u^{n+1}_{j,k})^2 + (v^{n+1}_{j,k})^2\Big) - \sum_{i=1}^{N} q_i (z_i)^n_{j,k}\right]. \tag{4.18}$$

We would like to point out that according to the ADP strategy, the old value $(z_1)^n_{j,k}$ and $(z_1)^n_{j,k}$—not $(z_1)^*_{j,k}$ and $(z_2)^*_{j,k}$—are used in both (4.16) and (4.18). Finally, the new values of z_3 are obtained using (4.13):

$$(z_3)^{n+1}_{j,k} = c_{j,k} - \frac{2W_3}{W_1}(z_1)^{n+1}_{j,k} + \frac{4W_3}{W_2}(z_2)^{n+1}_{j,k},$$

where the time-idependent quantities $c_{j,k}$ are given by

$$c_{j,k} = (z_3)^0_{j,k} + \frac{2W_3}{W_1}(z_1)^0_{j,k} - \frac{4W_3}{W_2}(z_2)^0_{j,k},$$

the new values of z_4 are obtained from (4.7):

$$(z_4)^{n+1}_{j,k} = 1 - (z_1)^{n+1}_{j,k} - (z_2)^{n+1}_{j,k} - (z_3)^{n+1}_{j,k} - (z_5)^{n+1}_{j,k},$$

and the values of z_5 remain unchanged, namely, $(z_5)^{n+1}_{j,k} = (z_5)^0_{j,k}$.

Remark 4.1 *We would like to stress that if the values of $(z_1)^*_{j,k}$ and $(z_2)^*_{j,k}$ are used in (4.18), this will cause the computed detonation waves to propagate with a nonphysical speed. It should be also observed that a formal consistency consideration would require one to use the values of z from the time level $t = t^n$, $(z_1)^n_{j,k}$ and $(z_1)^n_{j,k}$, in (4.17) instead of $(z_1)^*_{j,k}$ and $(z_2)^*_{j,k}$. However, the ADP strategy dictates one to use (4.17) in its current form as otherwise detonation waves propagating with nonphysical speeds will be captured by the resulting numerical method. The robustness of the proposed ODE solver as well as the failure of its aforementioned alternatives is demonstrted in Example 8c below.*

In addition, we note that the special ODE solver presented in this section can be used in a single species case, while the trapezoidal-like method presented in §3 may fail; see Example 8c.

4.3 Numerical Examples

In order to illusrtate the performance of the ADP methods for multispecies detonation, we conduct several numerical experiments in both 1-D and 2-D cases. As in §3.1, the 2-D ADP methods proposed in §4.1 and 4.2 can be reduced to their corresponding 1-D versions in a straightforward manner. In all of the following numerical examples, the CFL values are chosen as 0.3, except for Example 8a, where a smaller CFL value 0.1 is used to reduce the numerical oscillations that appear when larger CFL values are used.

Example 7—One Reaction

We begin with a multispecies case with one reaction

$$CH_4 + 2O_2 \to CO_2 + 2H_2O,$$

also studied in [3]. Here, $M=1$, $N=4$, $W_1=16$, $W_2=32$, $W_3=44$, $W_4=18$, $v'_{1,1}=1$, $v'_{2,1}=2$, $v'_{3,1}=0$, $v'_{4,1}=0$, $v''_{1,1}=0$, $v''_{2,1}=0$, $v''_{3,1}=1$ and $v''_{4,1}=2$, and formula (4.2) reads as

$$S_1=-\frac{1}{1024}K(\tau;\varepsilon_1,\tau_1)(\rho z_1)(\rho z_2)^2,\quad S_2=4S_1,\quad S_3=-\frac{11}{4}S_1. \tag{4.19}$$

Note that it is unnecessary to compute the source term S_4, since z_4 can be obtained directly from (4.3) and it is equal to $z_4=1-z_1-z_2-z_3$. We note that in the stiff case considered in Examples 7c and 7d, one only needs to compute S_1 since (4.19) immediately implies that $(z_2)_t-4(z_1)_t=0$ and $(z_3)_t+\frac{11}{4}(z_1)_t=0$. In Examples 7a–7d, we use the same parameters as in [3]: $\gamma=1.4$, $q_2=0$, $q_3=0$, $q_4=0$, $\tau_1=2$ and $q_1=500$ (in Examples 7a and 7c) or $q_1=100$ (in Examples 7b and 7d).

Example 7a—1-D Extremely Stiff Case

We begin with a 1-D extremely stiff case. The initial data are given by

$$(\rho,u,p,z_1,z_2,z_3,z_4)(x,0)=\begin{cases}(2,\,10,\,40,\,0,\,0.2,\,0.475,\,0.325), & \text{if } x\le 2.5,\\ (1,0,1,0.1,\,0.6,\,0.2,\,0.1), & \text{if } x>2.5.\end{cases} \tag{4.20}$$

In this example, we use the following ADP operator:

$$(z_i)_j^{n+1}=\begin{cases}z_i^{HT}, & \text{if } \tau_j^{n+1}\ge\tau_1,\\ z_i^{LT}, & \text{if } \tau_j^{n+1}<\tau_1,\end{cases}\qquad i=1,2,3, \tag{4.21}$$

with $z_1^{HT}=0$, $z_1^{LT}=0.1$, $z_2^{HT}=0.2$, $z_2^{LT}=0.6$, $z_3^{HT}=0.475$, $z_3^{LT}=0.2$, and $(z_4)_j^{n+1}=1-(z_1)_j^{n+1}-(z_2)_j^{n+1}-(z_3)_j^{n+1}$. Here, $(\cdot)_j^{n+1}$ denotes the value of the corresponding variable in the 1-D cell C_j at time level $t=t^{n+1}$. We compute the numerical solution using both the ADP and SDP methods on the domain $[0,50]$ using a uniform mesh with $\Delta x=0.25$ until the final time $t=3$. The numerical results (density, pressure, temperature and mass fractions of CH_4) are presented in Figure 4.1 along with the reference solution computed by the ADP method using a uniform spatial mesh with $\Delta x=0.025$. As one can observe, the solution consists of a detonation wave followed by a contact discontinuity and a shock, all captured accurately by the ADP method. We note that the ADP results are in good agreement with those reported in [3, Example 5.3], while the solution computed by the SDP method is incorrect.

Example 7b—2-D Extremely Stiff Case

We now consider the 2-D extremely stiff case with the radially symmetric initial data

$$(\rho,u,v,p,z_1,z_2,z_3,z_4)(x,y,0)=\begin{cases}(2,u_{\rm in}(x,y),v_{\rm in}(x,y),40,0,0.2,0.475,0.325), & \text{if } r\le 10,\\ (1,0,0,1,0.1,0.6,0.2,0.1), & \text{if } r>10,\end{cases}$$

where $r=\sqrt{x^2+y^2}$, $u_{\rm in}(x,y)=10x/r$ and $v_{\rm in}(x,y)=10y/r$. As in Example 7a, the ADP operator is given by

$$(z_i)_{j,k}^{n+1}=\begin{cases}z_i^{HT}, & \text{if } \tau_{j,k}^{n+1}\ge\tau_1,\\ z_i^{LT}, & \text{if } \tau_{j,k}^{n+1}<\tau_1,\end{cases}\qquad i=1,2,3$$

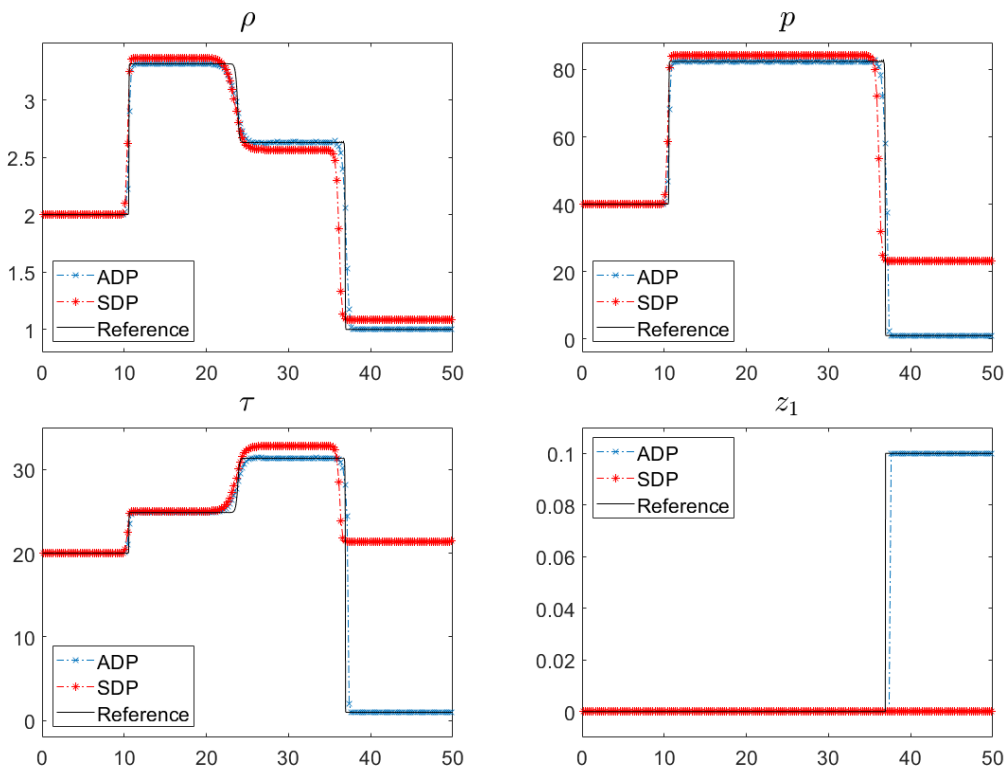

Figure 4.1: Example 7a: Density (ρ), pressure (p), temperature (τ) and mass fraction of CH_4 (z_1) computed by the ADP and SDP methods.

with $z_1^{HT} = 0$, $z_1^{LT} = 0.1$, $z_2^{HT} = 0.2$, $z_2^{LT} = 0.6$, $z_3^{HT} = 0.475$, $z_3^{LT} = 0.2$, and $(z_4)_{j,k}^{n+1} = 1 - (z_1)_{j,k}^{n+1} - (z_2)_{j,k}^{n+1} - (z_3)_{j,k}^{n+1}$. We solve this problem on the domain $[0, 50] \times [0, 50]$ using a uniform mesh with $\Delta x = \Delta y = 0.5$. Solid wall boundary conditions are imposed along $x = 0$ and $y = 0$, while the free boundary conditions are used along the other parts of the boundary. Figure 4.2 shows the pressure, temperature and mass fraction of CH_4 (we plot $100z_1$ rather then z_1 for a better visualization) along the line $y = x$, $x \geq 0$ at times $t = 1$, 2, 4 and 6 obtained by the ADP method. As one can see, our results are in good agreement with those reported in [3, Example 5.5]. We note that in this example, the SDP yields quite accurate results (very close to those shown in Figure 4.2), which are omitted for the sake of brevity.

Example 7c—1-D Stiff Case

We now turn our attention to the stiff case, in which we numerically integrate the ODE for z_1 (using the ODE solver similar to the one described in §4.2) instead of using the ADP operator (4.21). We use the same initial conditions (4.20) as in Example 7a.

We first take a very large value of $1/\varepsilon_1 = 2 \times 10^5$ and compute the solutions by both ADP and SDP methods on the domain $[0, 50]$ using a uniform mesh with $\Delta x = 0.25$ until the final time $t = 3$. The obtained results (density, pressure, temperature and mass fraction of CH_4) are presented in Figure 4.3 along with the reference solution, which is computed by the ADP method using a much finer uniform mesh with $\Delta x = 0.025$. As one can see, the ADP results are almost the same as the corresponding ADP results obtained in the extremely stiff case; see Figure 4.1. At the same time, the SDP results are still not accurate. We also notice that when the ODE for

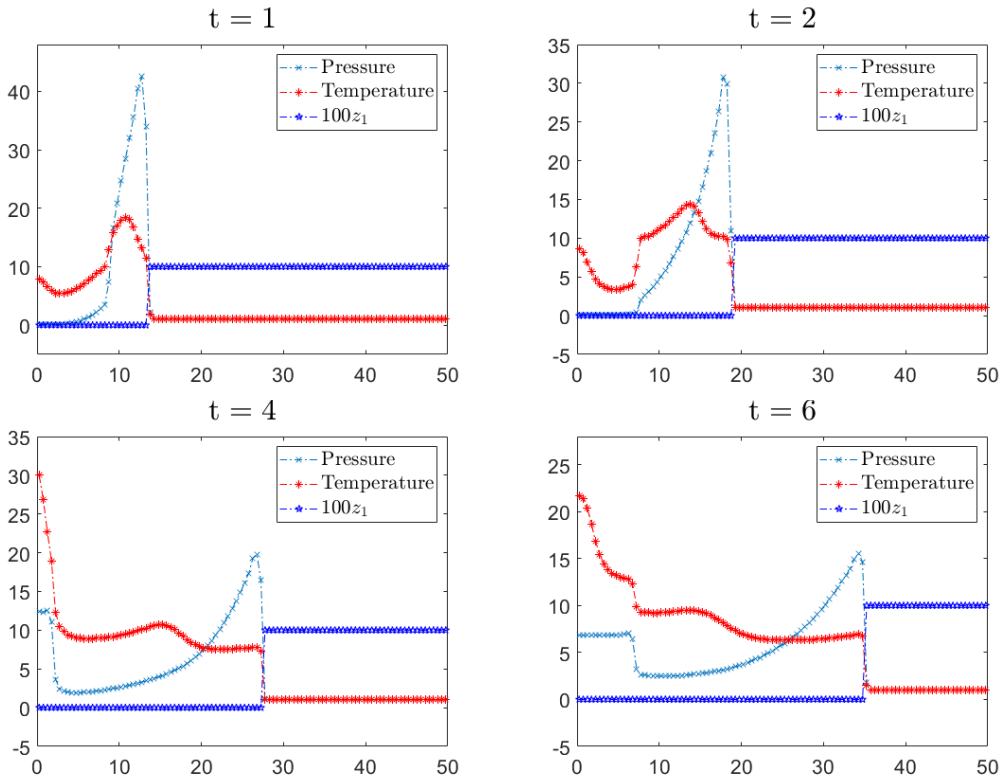

Figure 4.2: Example 7b: Pressure (p), temperature (τ) and 100 times of mass fraction of CH_4 ($100z_1$) computed by the ADP method at different times.

z_1 is numerically solved, the spiky structure of the detonation wave is more accurately resolved in the reference solution.

We then take a substantially smaller value of $1/\varepsilon_1 = 10^4$, repeat the same computations, and plot the obtained results in Figure 4.4. As one can see, the detonation waves captured by the ADP and SDP methods now propagate with about the same speed (with the SDP speed being still slightly larger), but the ADP method resolves the spiky structure of the detonation wave much better than its SPD counterpart.

Example 7d—2-D Stiff Case

Next, we consider the 2-D stiff case with precisely the same setting as the one used in Example 7b with the only exception that we now set $1/\varepsilon_1 = 2 \times 10^5$. The pressure, temperature and 100 times the mass fraction of the first species CH_4 computed by the ADP method at times $t = 1$, 2, 4 and 6 are shown in Figure 4.5, where one can see their slice across the line $y = x$, $x \geq 0$. As one can see, the numerical results almost coincide with those obtained in the extremely stiff case considered in Example 7b.

Example 8—Two Reactions

In this example taken from [3, 37], we simulate the two reaction–five species model (4.1)–(4.4) for the reactions (4.5). The details of the model as well as the corresponding ADP methods are

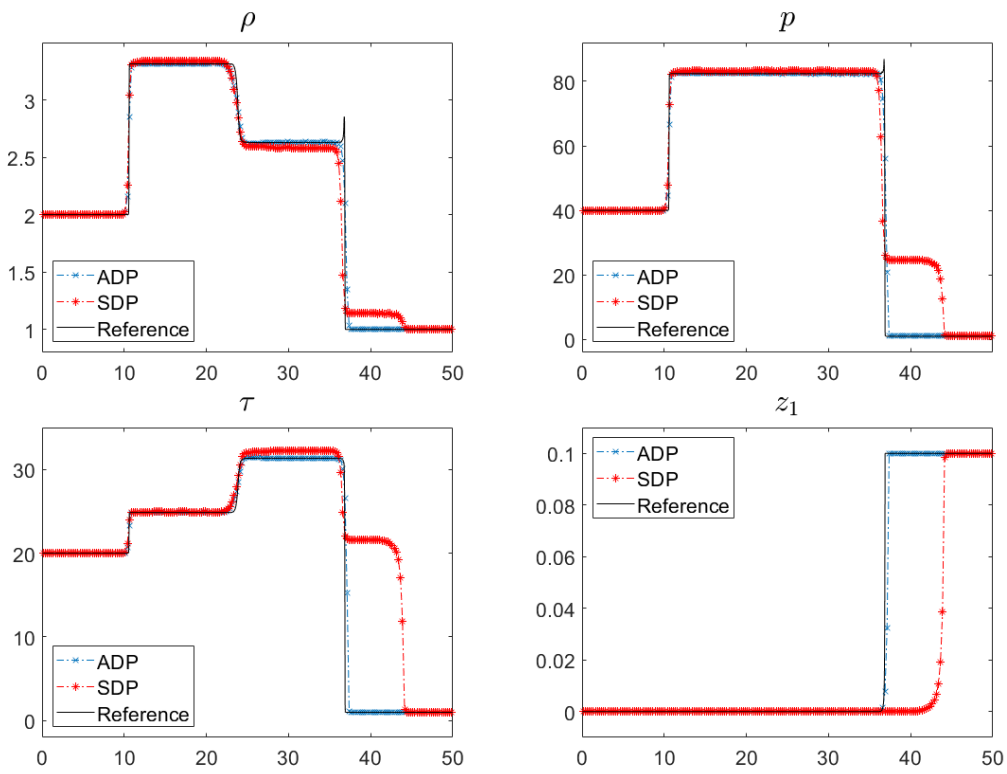

Figure 4.3: Example 7c: Density (ρ), pressure (p), temperature (τ) and mass fraction of CH_4 (z_1) computed by the ADP and SDP methods for $1/\varepsilon_1 = 2 \times 10^5$.

described and studied in §4. In Examples 8a–8d, we use the following parameters: $\gamma = 1.4$, $q_1 = 0$, $q_2 = 0$, $q_4 = -100$, $q_5 = 0$. Other parameters vary and will be specified in each particular example.

Example 8a—1-D Extremely Stiff Case

We begin with the 1-D extremely stiff case studied subject to the following Riemann initial data also used in [3, Example 5.4]:

$$(\rho, u, p, z_1, z_2, z_3, z_4, z_5)(x, 0) = \begin{cases} (2,\ 10,\ 40,\ 0,\ 0,\ 0.17,\ 0.63,\ 0.2), & \text{if } \ x \le 2.5, \\ (1, 0, 1,\ 0.08,\ 0.72,\ 0,\ 0,\ 0.2), & \text{if } \ x > 2.5. \end{cases}$$

In this example, we set $q_3 = -20$, $\tau_1 = 2$, $\tau_2 = 10$, and use the 1-D version of the ADP operator (4.9) with $z_1^{HT} = 0$, $z_1^{IT} = 0.035$, $z_1^{LT} = 0.08$, $z_2^{HT} = 0$, $z_2^{IT} = 0$, $z_2^{LT} = 0.72$, $z_3^{HT} = 0.17$, $z_3^{IT} = 0.765$ and $z_3^{LT} = 0$. We compute the numerical solution by both the ADP and SDP methods in the computational domain $[0, 50]$ using a uniform mesh with $\Delta x = 0.25$ until the final time $t = 3$. The numerical results (density, pressure, temperature and mass fractions of H_2) are presented in Figure 4.6 along with the reference solution computed by the ADP method using a much finer uniform mesh with $\Delta x = 0.025$. In this example, we only show the solution obtained by the ADP method as the results computed by the SDP method are practically the same. As one can observe, the results are in good agreement with those reported in [3, Example 5.4] except that the density and temperature fields plotted in [3, Figure 4] are smeared (this causes the pressure

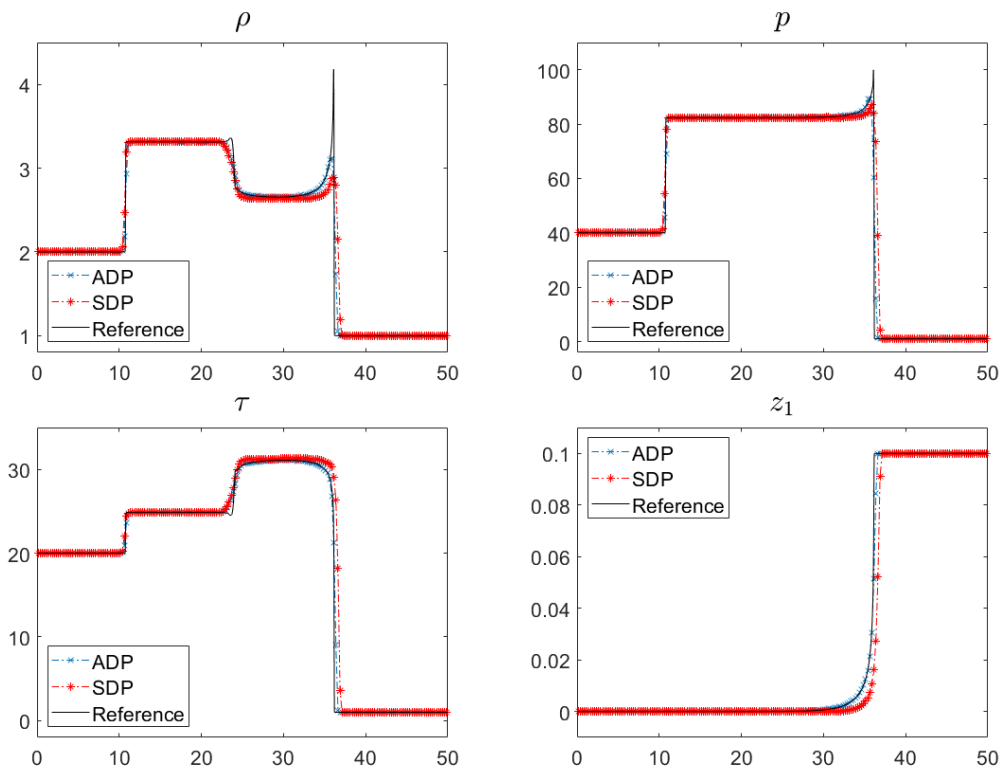

Figure 4.4: Example 7c: Same as in Figure 4.3, but for $1/\varepsilon_1 = 10^4$.

graph to be nonflat in the area $x \in [20, 30]$) compared with our much sharper jumps in ρ and τ and flat p around $x \in [20, 30]$.

Example 8b—2-D Extremely Stiff Case

We now consider the 2-D extremely stiff case with the initial data taken from [3, Example 5.6]:

$$(\rho, u, v, p, z_1, z_2, z_3, z_4, z_5)(x, y, 0) = \begin{cases} (2, 10, 0, 40, 0, 0, 0.17, 0.63, 0.2), & \text{if } r \le \xi(y), \\ (1, 0, 0, 1, 0.08, 0.72, 0, 0, 0.2), & \text{if } r > \xi(y), \end{cases}$$

where $r = \sqrt{x^2 + y^2}$ and

$$\xi(y) = \begin{cases} 12.5 - |y - 12.5|, & \text{if } |y - 12.5| \le 7.5, \\ 5, & \text{if } |y - 12.5| > 7.5. \end{cases}$$

In this example, we set $q_3 = -40$, $\tau_1 = 2$, $\tau_2 = 10$, and use the ADP operator (4.9) with the same projection mass fraction values, which were used in Example 8a, namely, $z_1^{HT} = 0$, $z_1^{IT} = 0.035$, $z_1^{LT} = 0.08$, $z_2^{HT} = 0$, $z_2^{IT} = 0$, $z_2^{LT} = 0.72$, $z_3^{HT} = 0.17$, $z_3^{IT} = 0.765$ and $z_3^{LT} = 0$. The problem is solved in the computational domain $[0, 150] \times [0, 25]$ using a uniform mesh with $\Delta x = \Delta y = 0.5$. Solid wall boundary conditions are implemented along the boundaries $y = 0$ and $y = 25$, and free boundary conditions are used at $x = 0$ and $x = 150$. In Figure 4.7, we show contour plots of the density computed by both the ADP and SDP methods at times $t = 2$, 4, 6 and 8. We also plot, in Figure 4.8, profiles of pressure, temperature and 300 times mass fraction of H_2 (as before, we plot

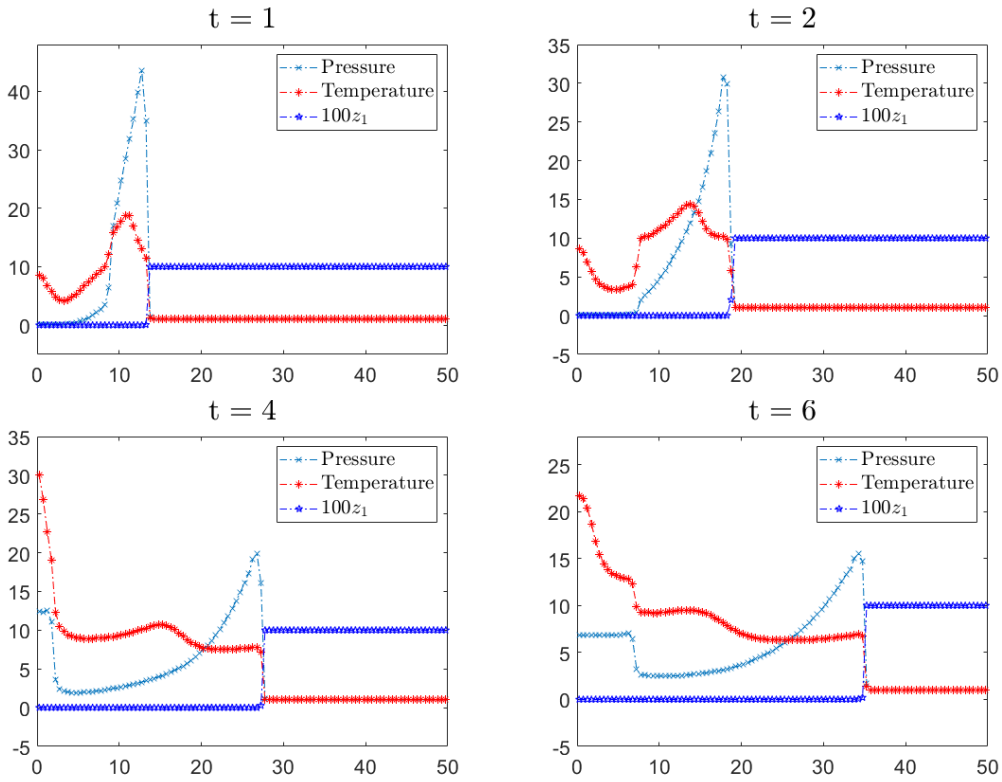

Figure 4.5: Example 7d: Pressure (p), temperature (τ) and 100 times of mass fraction of CH_4 ($100z_1$) computed by the ADP method at different times.

$300z_1$ rather then z_1 for a better visualization) along the line $y = 12.5$ at the same times. As one can clearly see from these figures, the ADP and SDP solutions are very different in this example. As the ADP solution agrees well with the one reported in [3, Example 5.6], we conclude that the ADP method capture the detonation wave propagating with the correct speeds.

Example 8c—1-D Stiff Case

Next, we study the 1-D stiff case using an example similar to the one considered in [37]. We take the following Riemann initial data:

$$(\rho, u, p, z_1, z_2, z_3, z_4, z_5)(x, 0) = \begin{cases} (2,\ 10,\ 40,\ 0,\ 0,\ 0.17,\ 0.63,\ 0.2), & \text{if } \ x \le 0.5, \\ (1, 0, 1,\ 0.08,\ 0.72,\ 0,\ 0,\ 0.2), & \text{if } \ x > 0.5, \end{cases}$$

and the parameters $q_3 = -100$, $\tau_1 = \tau_2 = 1.5$ and $1/\varepsilon_1 = 1/\varepsilon_2 = 10^5$. We compute the solution until the final time $t = 0.06$ by both the ADP and SDP methods on the domain $[0, 2]$ using a uniform mesh with $\Delta x = 1/150$ and present the obtained results (pressure, temperature, mass fractions of H_2 and OH) in Figure 4.9. We also show the reference solution, which was computed by the ADP method with a much finer uniform spatial with mesh $\Delta x = 1/1500$. As can be clearly seen, only the ADP method captures the detonation wave propagating with the correct speed showing a good agreement with the numerical solution reported in [37, Example 5.3].

As pointed out in Remark 4.1, it is important to numerically solve the ODE system (4.10)–(4.12) using a special ODE solver presented in §4.2. We now test the two alternative ODE solvers

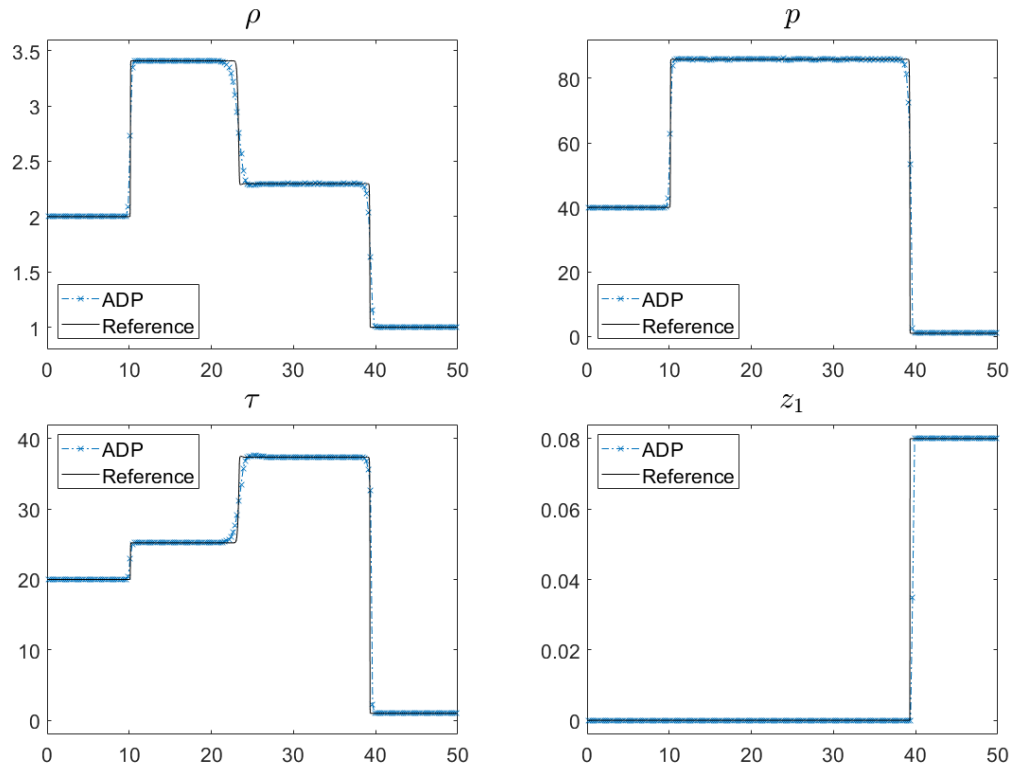

Figure 4.6: Example 8a: Density (ρ), pressure (p), temperature (τ) and mass fraction of H_2 (z_1) computed by the ADP method.

mentioned in Remark 4.1. The first alternative ODE solver is obtained by replacing $(z_1^*)_{j,k}$ and $(z_2^*)_{j,k}$ with $(z_1^n)_{j,k}$ and $(z_2^n)_{j,k}$, respectively, in the formulae in (4.17). The results computed using this ODE solver are shown in Figure 4.10. One can observe a small difference in the captured z_1 and z_3 compared to Figure 4.9: the mass fractions of H_2 and OH have small jumps at $x = 0.5$, which is the breaking point in the initial data. Moreover, we conduct a numerical experiment with precisely the same setting but smaller values $1/\varepsilon_1 = 1/\varepsilon_2 = 5 \times 10^4$, and observe even bigger jumps in the mass fractions; see Figure 4.11. We have also performed similar numerical experiments with the second alternative ODE solver mentioned in Remark 4.1—the trapezoidal-like method presented in §3—and the obtained results, omitted here for the sake of brevity, have been very similar to those reported in Figures 4.10 and 4.11.

Example 8d—2-D Stiff case

In the last example, we consider the 2-D case with the radially symmetric initial data given by

$$(\rho, u, v, p, z_1, z_2, z_3, z_4, z_5)(x, y, 0) = \begin{cases} (2, u_{\text{in}}(x, y), v_{\text{in}}(x, y), 40, 0, 0, 0.17, 0.63, 0.2), & \text{if } r \le 2, \\ (1, 0, 0, 1, 0.08, 0.72, 0, 0, 0.2), & \text{if } r > 2, \end{cases}$$

where $r = \sqrt{x^2 + y^2}$, $u_{\text{in}}(x, y) = 10x/r$ and $v_{\text{in}}(x, y) = 10y/r$. Other parameters are as the same as these in Example 8c: $q_3 = -100$, $\tau_1 = \tau_2 = 1.5$ and $1/\varepsilon_1 = 1/\varepsilon_2 = 10^5$. We compute the solution until the final time $t = 0.06$ by both the ADP and SDP methods in the computational domain $[-5, 5] \times [0, 5]$ using a uniform mesh with $\Delta x = \Delta y = 0.025$. The solid wall boundary conditions

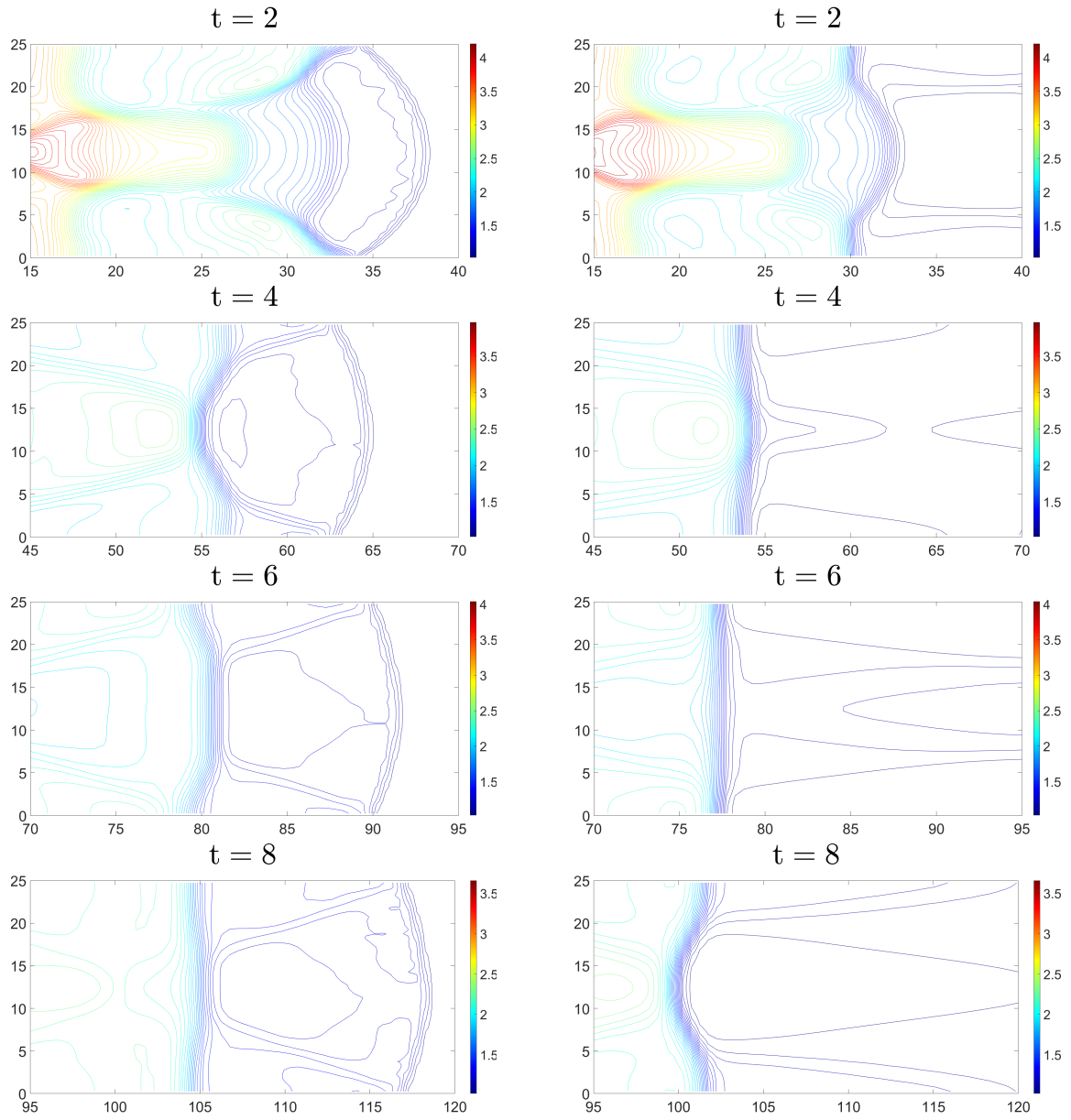

Figure 4.7: Example 8b: Contour plots of density (ρ) computed by the ADP (left column) and SDP (right column) methods at different times.

are used along the bottom part of the domain, while the free boundary conditions are implemented at the other parts of the boundary. Contour plots of the density, pressure, temperature and mass fraction of H_2 are presented in Figure 4.12. As one can clearly see, the results obtained by the ADP and SDP methods are very different. As in previous example, the detonation wave computed by the SDP method propagates much faster than the one captured by the proposed ADP method.

Acknowledgment: The work of A. Chertock was supported in part by NSF grant DMS-1818684. The work of A. Kurganov was supported in part by NSFC grants 11771201 and 1201101343, and by the fund of the Guangdong Provincial Key Laboratory of Computational Science and Material

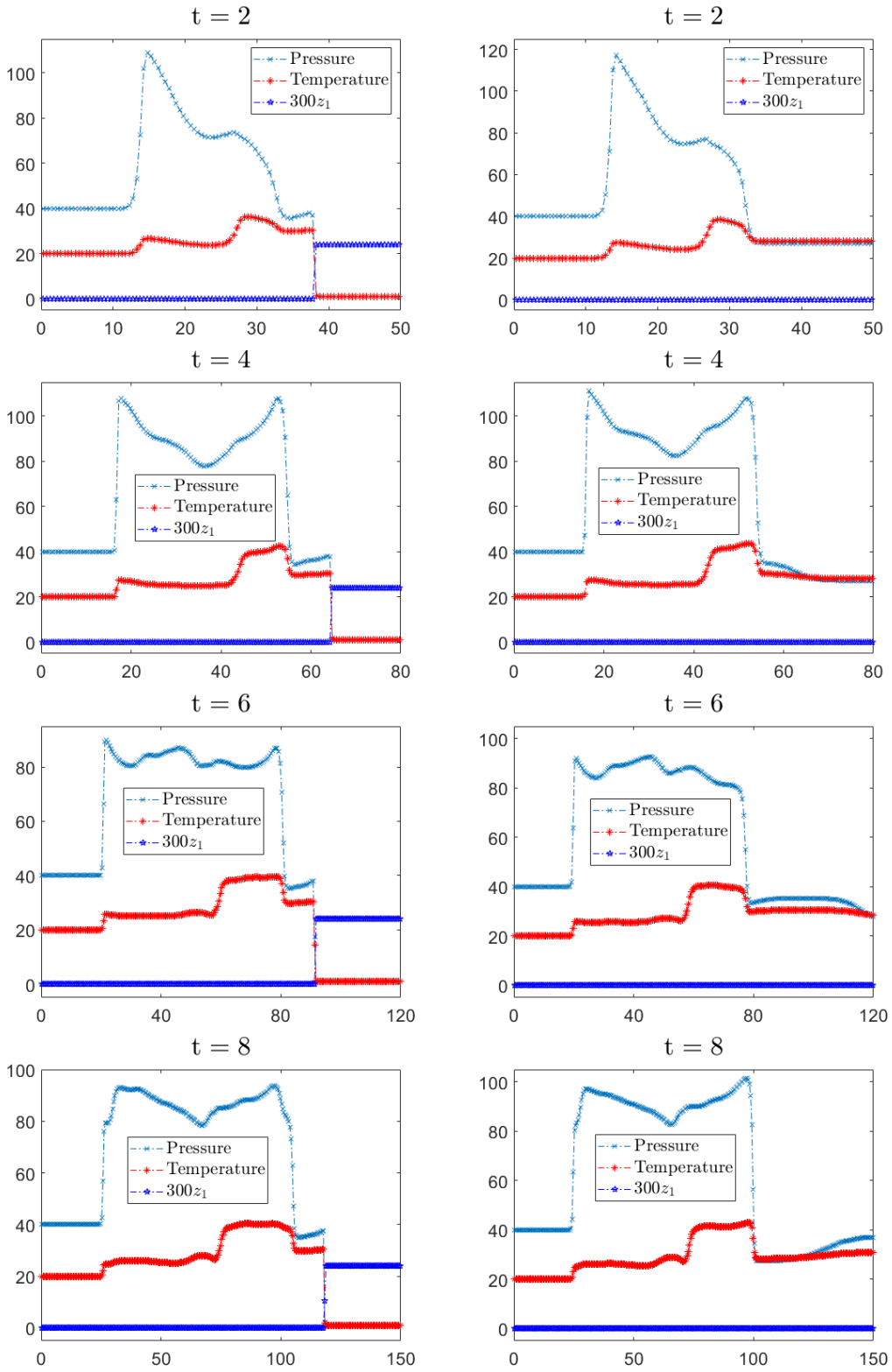

Figure 4.8: Example 8b: Pressure (p), temperature (τ) and 300 times mass fraction of H_2 ($300z_1$) computed by the ADP (left column) and SDP (right column) methods at different times.

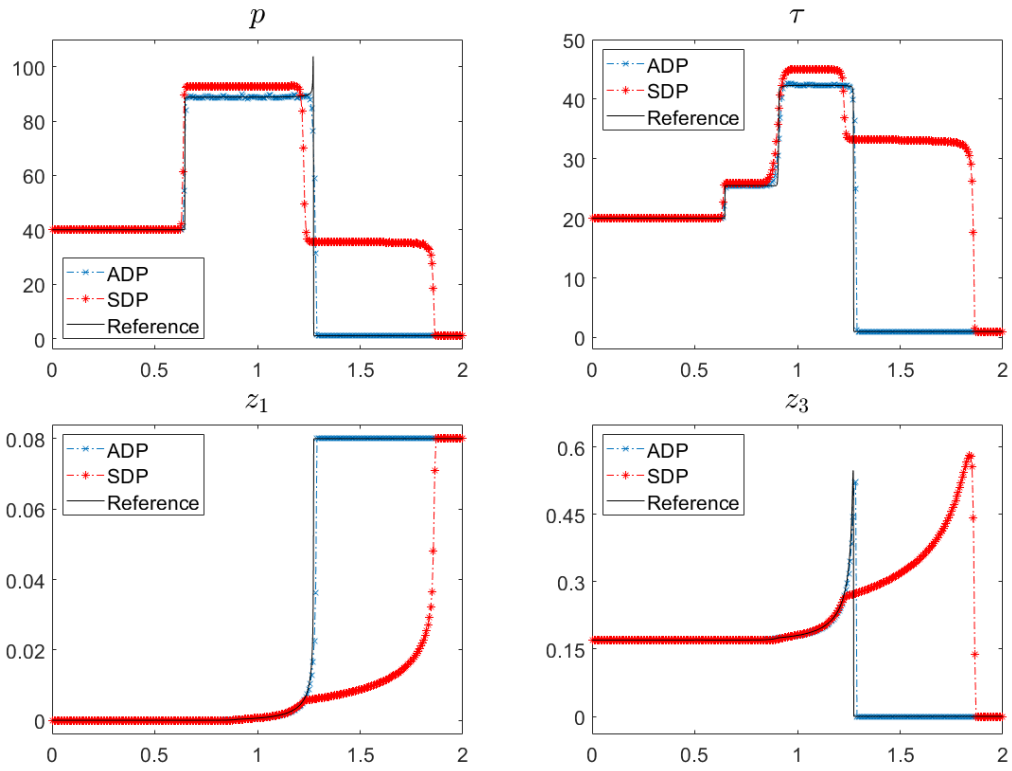

Figure 4.9: Example 8c: Pressure (p), temperature (τ), mass fraction of H_2 (z_1) and mass fraction of OH (z_3) computed by the ADP and SDP methods.

Design (No. 2019B030301001).

A Semi-Discrete Central-Upwind Scheme

In this section, we briefly describe the semi-discrete central-upwind scheme for the homogeneous 2-D systems (2.1), (1.3) and (2.4), (1.3). The 2-D semi-discrete central-upwind scheme from [26] admits the following flux form:

$$\frac{\mathrm{d}}{\mathrm{d}t}\overline{\boldsymbol{U}}_{j,k}(t)=-\frac{\boldsymbol{H}^x_{j+\frac12,k}-\boldsymbol{H}^x_{j-\frac12,k}}{\Delta x}-\frac{\boldsymbol{H}^y_{j,k+\frac12}-\boldsymbol{H}^y_{j,k-\frac12}}{\Delta y}, \tag{A.1}$$

where the numerical fluxes are

$$\begin{aligned}
\boldsymbol{H}^x_{j+\frac12,k}&=\frac{a^+_{j+\frac12,k}\boldsymbol{F}(\boldsymbol{U}^{\mathrm{E}}_{j,k})-a^-_{j+\frac12,k}\boldsymbol{F}(\boldsymbol{U}^{\mathrm{W}}_{j+1,k})}{a^+_{j+\frac12,k}-a^-_{j+\frac12,k}}+\frac{a^+_{j+\frac12,k}a^-_{j+\frac12,k}}{a^+_{j+\frac12,k}-a^-_{j+\frac12,k}}\left[\boldsymbol{U}^{\mathrm{W}}_{j+1,k}-\boldsymbol{U}^{\mathrm{E}}_{j,k}\right],\\
\boldsymbol{H}^y_{j,k+\frac12}&=\frac{b^+_{j,k+\frac12}\boldsymbol{G}(\boldsymbol{U}^{\mathrm{N}}_{j,k})-b^-_{j,k+\frac12}\boldsymbol{G}(\boldsymbol{U}^{\mathrm{S}}_{j,k+1})}{b^+_{j,k+\frac12}-b^-_{j,k+\frac12}}+\frac{b^+_{j,k+\frac12}b^-_{j,k+\frac12}}{b^+_{j,k+\frac12}-b^-_{j,k+\frac12}}\left[\boldsymbol{U}^{\mathrm{N}}_{j,k+1}-\boldsymbol{U}^{\mathrm{S}}_{j,k}\right].
\end{aligned} \tag{A.2}$$

The quantities $\overline{\boldsymbol{U}}_{j,k}$, $\boldsymbol{H}^x_{j,k}$, $\boldsymbol{H}^y_{j,k}$, $a^+_{j,k}$, $a^-_{j,k}$, $\boldsymbol{U}^{\mathrm{E}}_{j,k}$, $\boldsymbol{U}^{\mathrm{W}}_{j,k}$, $\boldsymbol{U}^{\mathrm{N}}_{j,k}$ and $\boldsymbol{U}^{\mathrm{S}}_{j,k}$ depend in fact on t, but we suppress this dependence for the sake of brevity.

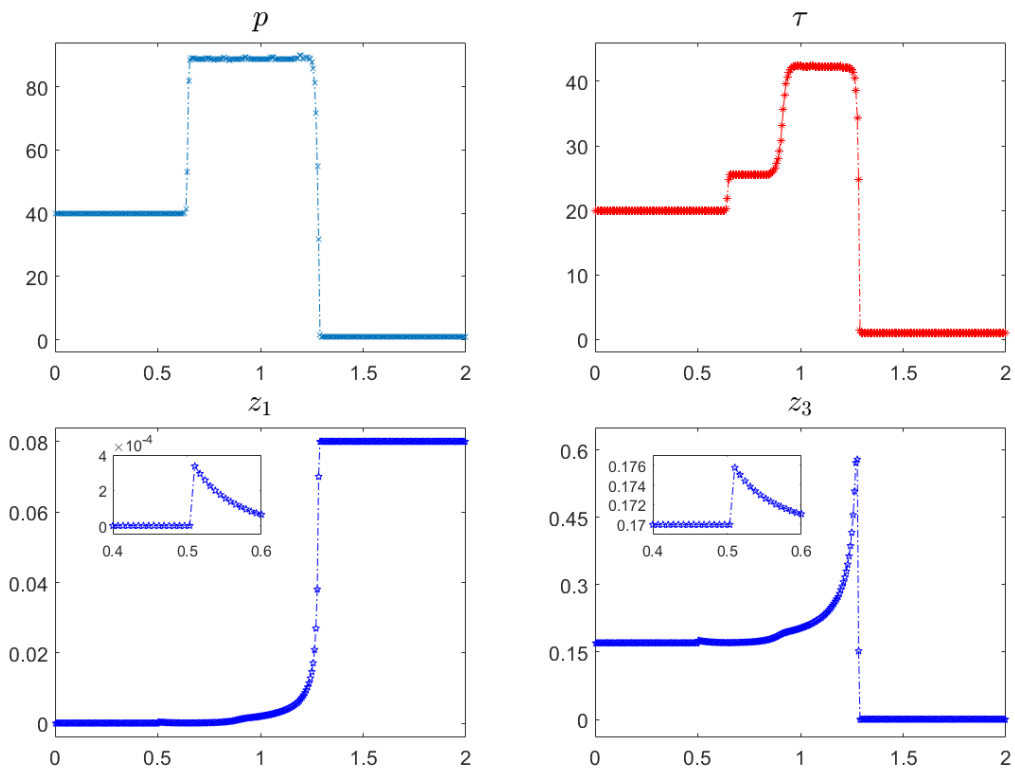

Figure 4.10: Example 8c: Pressure (p), temperature (τ), mass fraction of H_2 (z_1) and mass fraction of OH (z_3) computed by the ADP method with the alternative ODE solver obtained by replacing $(z_1^*)_{j,k}$ and $(z_2^*)_{j,k}$ with $(z_1^n)_{j,k}$ and $(z_2^n)_{j,k}$, respectively, in (4.17). The plots of z_1 and z_3 contain zooms at the area of small jumps occuring at $x = 0.5$.

In (A.2),

$$\boldsymbol{U}^{\rm E}_{j,k} = \overline{\boldsymbol{U}}_{j,k} + \frac{\Delta x}{2}(\boldsymbol{U}_x)_{j+\frac{1}{2},k}, \qquad \boldsymbol{U}^{\rm W}_{j,k} = \overline{\boldsymbol{U}}_{j,k} - \frac{\Delta x}{2}(\boldsymbol{U}_x)_{j+\frac{1}{2},k},$$
$$\boldsymbol{U}^{\rm N}_{j,k} = \overline{\boldsymbol{U}}_{j,k} + \frac{\Delta y}{2}(\boldsymbol{U}_y)_{j,k+\frac{1}{2}}, \qquad \boldsymbol{U}^{\rm S}_{j,k} = \overline{\boldsymbol{U}}_{j,k} - \frac{\Delta y}{2}(\boldsymbol{U}_y)_{j,k+\frac{1}{2}}$$

are the point values of the piecewise linear reconstruction

$$\widetilde{\boldsymbol{U}}(x,y) = \overline{\boldsymbol{U}}_{j,k} + (\boldsymbol{U}_x)_{j,k}(x - x_j) + (\boldsymbol{U}_y)_{j,k}(y - y_k) \quad \text{for } (x,y) \in \left(x_{j-\frac{1}{2}}, x_{j+\frac{1}{2}}\right) \times \left(y_{k-\frac{1}{2}}, y_{k+\frac{1}{2}}\right)$$

at the midpoints of the edges of cell (j,k).

The numerical derivatives $(\boldsymbol{U}_x)_{j,k}$ and $(\boldsymbol{U}_y)_{j,k}$ are to be computed using a nonlinear limiter. We have used a minmod limiter (see, e.g., [30, 32, 34]), which gives

$$(\boldsymbol{U}_x)_{j,k} = \text{minmod}\left(\frac{\overline{\boldsymbol{U}}_{j+1,k} - \overline{\boldsymbol{U}}_{j,k}}{\Delta x}, \frac{\overline{\boldsymbol{U}}_{j,k} - \overline{\boldsymbol{U}}_{j-1,k}}{\Delta x}\right),$$
$$(\boldsymbol{U}_y)_{j,k} = \text{minmod}\left(\frac{\overline{\boldsymbol{U}}_{j,k+1} - \overline{\boldsymbol{U}}_{j,k}}{\Delta y}, \frac{\overline{\boldsymbol{U}}_{j,k} - \overline{\boldsymbol{U}}_{j,k-1}}{\Delta y}\right),$$

where the minmod function is defined as

$$\text{minmod}(a,b) := \frac{\text{sgn}(a) + \text{sgn}(b)}{2} \cdot \min(|a|, |b|).$$

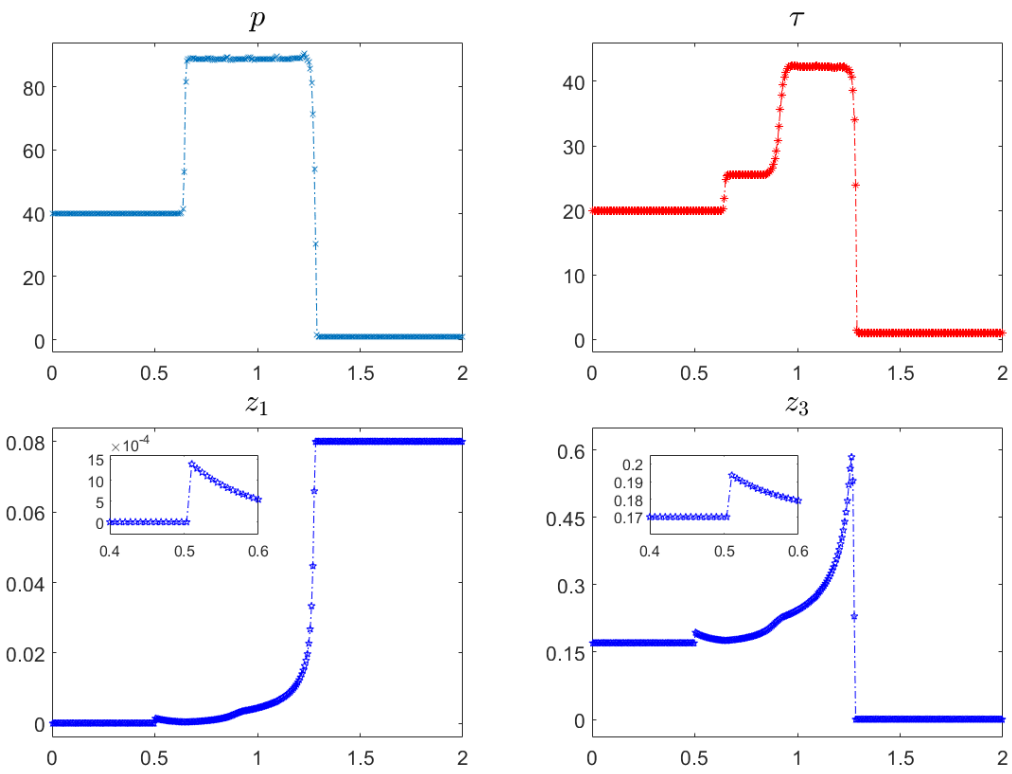

Figure 4.11: Example 8c: Same as in Figure 4.10, but for $1/\varepsilon_1 = 1/\varepsilon_2 = 5 \times 10^4$.

One-sided local propagation speeds in the x- and y-directions $a^{\pm}_{j+\frac{1}{2},k}$ and $b^{\pm}_{j,k+\frac{1}{2}}$ are obtained using the largest/smallest eigenvalues of the Jacobian. For the reactive Euler systems (2.1), (1.3) and (2.4), (1.3), we obtain

$$a^{+}_{j+\frac{1}{2},k} = \max\left(u^{\mathrm{E}}_{j,k} + \sqrt{\frac{\gamma p^{\mathrm{E}}_{j,k}}{\rho^{\mathrm{E}}_{j,k}}},\ u^{\mathrm{W}}_{j+1,k} + \sqrt{\frac{\gamma p^{\mathrm{W}}_{j+1,k}}{\rho^{\mathrm{W}}_{j,k}}},\ 0\right),$$

$$a^{-}_{j+\frac{1}{2},k} = \min\left(u^{\mathrm{E}}_{j,k} - \sqrt{\frac{\gamma p^{\mathrm{E}}_{j,k}}{\rho^{\mathrm{E}}_{j,k}}},\ u^{\mathrm{W}}_{j+1,k} - \sqrt{\frac{\gamma p^{\mathrm{W}}_{j+1,k}}{\rho^{\mathrm{W}}_{j,k}}},\ 0\right),$$

$$b^{+}_{j,k+\frac{1}{2}} = \max\left(u^{\mathrm{N}}_{j,k} + \sqrt{\frac{\gamma p^{\mathrm{N}}_{j,k}}{\rho^{\mathrm{N}}_{j,k}}},\ u^{\mathrm{S}}_{j,k+1} + \sqrt{\frac{\gamma p^{\mathrm{S}}_{j,k+1}}{\rho^{\mathrm{S}}_{j,k}}},\ 0\right),$$

$$b^{-}_{j,k+\frac{1}{2}} = \min\left(u^{\mathrm{N}}_{j,k} - \sqrt{\frac{\gamma p^{\mathrm{N}}_{j,k}}{\rho^{\mathrm{N}}_{j,k}}},\ u^{\mathrm{S}}_{j,k+1} - \sqrt{\frac{\gamma p^{\mathrm{S}}_{j,k+1}}{\rho^{\mathrm{S}}_{j,k}}},\ 0\right).$$

Finally, the ODE system (A.1) is numerically integrated by the three-stage third-order strong stability preserving (SSP) Runge-Kutta method; see, [13, 14].

References

[1] W. BAO AND S. JIN, *The random projection method for hyperbolic conservation laws with*

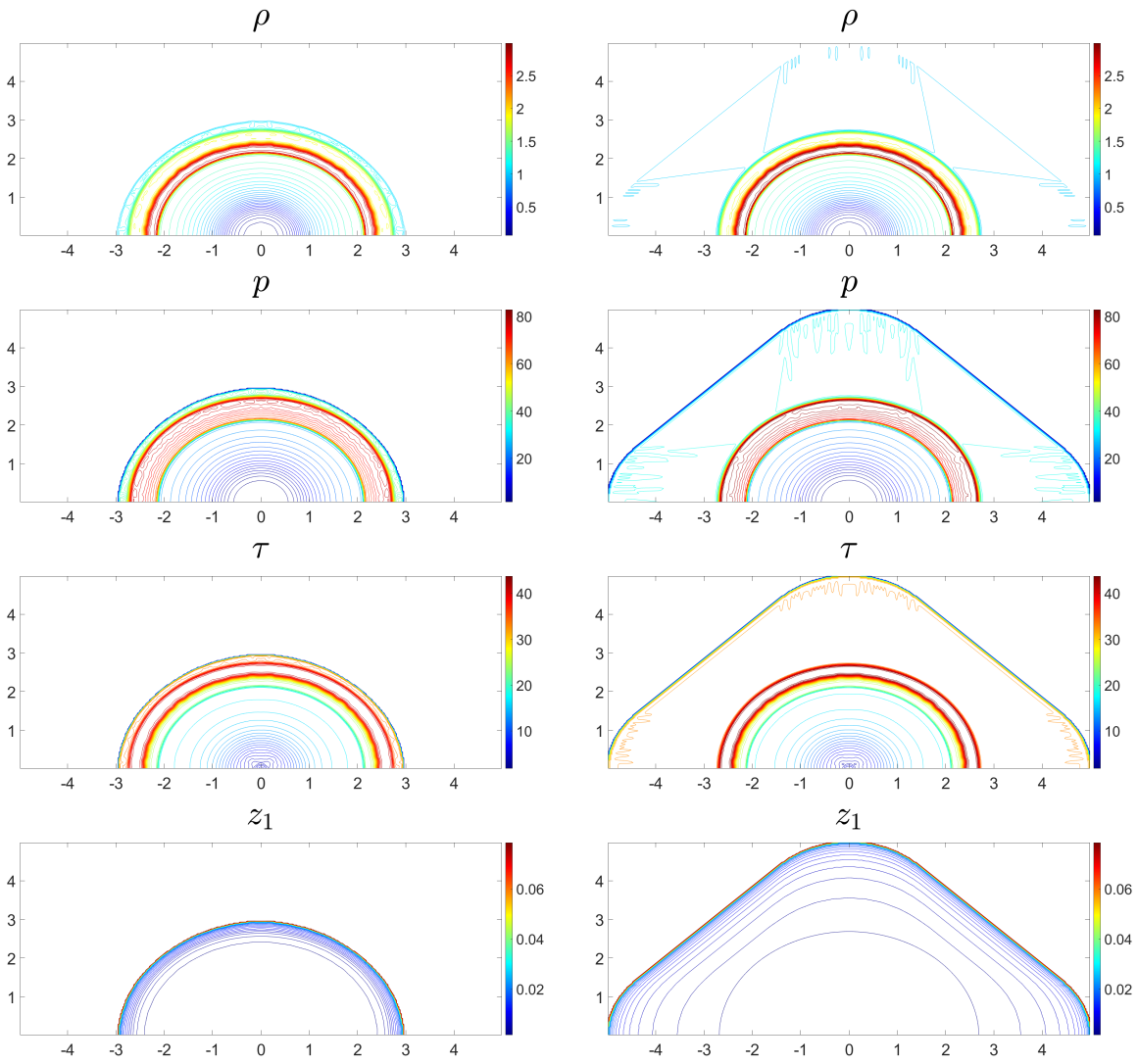

Figure 4.12: Example 8d: Density (ρ), pressure (p), temperature (τ) and mass fraction of H_2 (z_1) computed by the ADP (left column) and SDP (right column) methods.

stiff reaction terms, J. Comput. Phys., 163 (2000), pp. 216–248.

[2] W. BAO AND S. JIN, *The random projection method for stiff detonation capturing*, SIAM J. Sci. Comput., 23 (2001), pp. 1000–1026 (electronic).

[3] W. BAO AND S. JIN, *The random projection method for stiff multispecies detonation capturing*, J. Comput. Phys., 178 (2002), pp. 37–57.

[4] M. BEN-ARTZI, *The generalized Riemann problem for reactive flows*, J. Comput. Phys., 81 (1989), pp. 70–101.

[5] A. C. BERKENBOSCH, *Capturing detonation waves for the reactive Euler equations*, PhD thesis, Department of Mathematics and Computer Science, Technische Universiteit Eindhoven, 1995.

[6] A. C. Berkenbosch, E. F. Kaasschieter, and R. Klein, *Detonation capturing for stiff combustion chemistry*, Combust. Theory Model., 2 (1998), pp. 313–348.

[7] A. Bourlioux, A. J. Majda, and V. Roytburd, *Theoretical and numerical structure for unstable one-dimensional detonations*, SIAM J. Appl. Math., 51 (1991), pp. 303–343.

[8] A. Chertock and A. Kurganov, *On a practical implementation of particle methods*, Appl. Numer. Math., 56 (2006), pp. 1418–1431.

[9] A. J. Chorin, *Random choice methods with applications to reacting gas flow*, J. Comput. Phys., 25 (1977), pp. 253–272.

[10] P. Colella, A. Majda, and V. Roytburd, *Fractional step methods for reacting shock waves*, in Reacting flows: combustion and chemical reactors, Part 2 (Ithaca, N.Y., 1985), vol. 24 of Lectures in Appl. Math., Amer. Math. Soc., Providence, RI, 1986, pp. 459–477.

[11] P. Colella, A. Majda, and V. Roytburd, *Theoretical and numerical structure for reacting shock waves*, SIAM J. Sci. Statist. Comput., 7 (1986), pp. 1059–1080.

[12] R. P. Fedkiw, T. Aslam, and S. Xu, *The ghost fluid method for deflagration and detonation discontinuities*, J. Comput. Phys., 154 (1999), pp. 393–427.

[13] S. Gottlieb, D. Ketcheson, and C.-W. Shu, *Strong stability preserving Runge-Kutta and multistep time discretizations*, World Scientific Publishing Co. Pte. Ltd., Hackensack, NJ, 2011.

[14] S. Gottlieb, C.-W. Shu, and E. Tadmor, *Strong stability-preserving high-order time discretization methods*, SIAM Rev., 43 (2001), pp. 89–112.

[15] D. F. Griffiths, A. M. Stuart, and H. C. Yee, *Numerical wave propagation in an advection equation with a nonlinear source term*, SIAM J. Numer. Anal., 29 (1992), pp. 1244–1260.

[16] C. Helzel, R. J. Leveque, and G. Warnecke, *A modified fractional step method for the accurate approximation of detonation waves*, SIAM J. Sci. Comput., 22 (2000), pp. 1489–1510.

[17] W. D. Henshaw and D. W. Schwendeman, *An adaptive numerical scheme for high-speed reactive flow on overlapping grids*, J. Comput. Phys., 191 (2003), pp. 420–447.

[18] W. D. Henshaw and D. W. Schwendeman, *Moving overlapping grids with adaptive mesh refinement for high-speed reactive and non-reactive flow*, J. Comput. Phys., 216 (2006), pp. 744–779.

[19] P. Hwang, R. Fedkiw, B. Merriman, T. Aslam, A. Karagozian, and S. Osher, *Numerical resolution of pulsating detonation waves*, Combust. Theory Modelling, 4 (2000), pp. 217–240.

[20] A. Kurganov, *An accurate deterministic projection method for hyperbolic systems with stiff source term*, in Hyperbolic problems: theory, numerics, applications, Springer, Berlin, 2003, pp. 665–674.

[21] A. Kurganov, *An accurate deterministic projection method for hyperbolic systems with stiff source term*, in Hyperbolic problems: theory, numerics, applications, Springer, Berlin, 2003, pp. 665–674.

[22] A. Kurganov and C.-T. Lin, *On the reduction of numerical dissipation in central-upwind schemes*, Commun. Comput. Phys., 2 (2007), pp. 141–163.

[23] A. Kurganov, S. Noelle, and G. Petrova, *Semidiscrete central-upwind schemes for hyperbolic conservation laws and Hamilton-Jacobi equations*, SIAM J. Sci. Comput., 23 (2001), pp. 707–740.

[24] A. Kurganov, M. Prugger, and T. Wu, *Second-order fully discrete central-upwind scheme for two-dimensional hyperbolic systems of conservation laws*, SIAM J. Sci. Comput., 39 (2017), pp. A947–A965.

[25] A. Kurganov and E. Tadmor, *New high-resolution central schemes for nonlinear conservation laws and convection-diffusion equations*, J. Comput. Phys., 160 (2000), pp. 241–282.

[26] A. Kurganov and E. Tadmor, *Solution of two-dimensional Riemann problems for gas dynamics without Riemann problem solvers*, Numer. Methods Partial Differential Equations, 18 (2002), pp. 584–608.

[27] R. J. LeVeque and H. C. Yee, *A study of numerical methods for hyperbolic conservation laws with stiff source terms*, J. Comput. Phys., 86 (1990), pp. 187–210.

[28] M.-S. Liou, *A sequel to AUSM: AUSM$^+$*, J. Comput. Phys., 129 (1996), pp. 364–382.

[29] M.-S. Liou and C. J. Steffen, Jr., *A new flux splitting scheme*, J. Comput. Phys., 107 (1993), pp. 23–39.

[30] H. Nessyahu and E. Tadmor, *Nonoscillatory central differencing for hyperbolic conservation laws*, J. Comput. Phys., 87 (1990), pp. 408–463.

[31] R. B. Pember, *Numerical methods for hyperbolic conservation laws with stiff relaxation. I. Spurious solutions*, SIAM J. Appl. Math., 53 (1993), pp. 1293–1330.

[32] P. K. Sweby, *High resolution schemes using flux limiters for hyperbolic conservation laws*, SIAM J. Numer. Anal., 21 (1984), pp. 995–1011.

[33] L. Tosatto and L. Vigevano, *Numerical solution of under-resolved detonations*, J. Comput. Phys., 227 (2008), pp. 2317–2343.

[34] B. van Leer, *Towards the ultimate conservative difference scheme. V. A second-order sequel to Godunov's method*, J. Comput. Phys., 32 (1979), pp. 101–136.

[35] W. Wang, C.-W. Shu, H. C. Yee, and B. Sjögreen, *High order finite difference methods with subcell resolution for advection equations with stiff source terms*, J. Comput. Phys., 231 (2012), pp. 190–214.

[36] F. A. Williams, *Combustion Theory*, Addison-Wesley, Reading, MA, 1965.

[37] B. YU, L. LI, B. ZHANG, AND J. WANG, *An approach to obtain the correct shock speed for Euler equations with stiff detonation*, Commun. Comput. Phys., 22 (2017), pp. 259–284.

[38] B. ZHANG, H. LIU, F. CHEN, AND J. H. WANG, *The equilibrium state method for hyperbolic conservation laws with stiff reaction terms*, J. Comput. Phys., 263 (2014), pp. 151–176.